

博士論文

Excitonic Insulator Transition in the Zero-Gap

Semiconductor Ta_2NiSe_5

(ゼロギャップ半導体 Ta_2NiSe_5 における励起子絶縁体転移)

魯 楊帆

Thesis

**Excitonic Insulator Transition in the Zero-Gap
Semiconductor Ta₂NiSe₅**

School of Frontier Science, Department of Advanced Materials Science
The University of Tokyo

Yangfan LU (No. 47-127015)

Supervisor: Prof. Hidenori TAKAGI

Contents

Chapter 1 Introduction.....	6
1. 1 What is an excitonic insulator?.....	9
1. 2 Excitonic insulator candidate materials.....	12
1. 2. 1 $\text{TmSe}_{0.45}\text{Te}_{0.55}$	13
1. 2. 2 $1T\text{-TiSe}_2$	15
1. 2. 3 Issues in the existing excitonic insulator candidates.....	16
1. 3 A new excitonic insulator candidate Ta_2NiSe_5	20
1. 3. 1 The crystal and the band structures.....	20
1. 3. 2 Proposal for an excitonic insulator state in Ta_2NiSe_5	22
Chapter 2 Objective.....	25
2. 1 Basic physical properties of pure Ta_2NiSe_5	25
2. 2 Electronic phase diagram in Ta_2NiSe_5	26
Chapter 3 Experimental.....	30
3. 1 Sample preparation and characterization of Ta_2NiCh_5 ($Ch = \text{sulfur, selenium and tellurium}$).....	30
3. 2 Sample preparation and characterization of $\text{Ta}_2\text{Pd}_x\text{S}_5$	31
3. 3 Transport, optical and thermodynamic properties.....	32
Chapter 4 Basic physical properties of Ta_2NiSe_5	35
4. 1 Anisotropic in-plane resistivity in Ta_2NiSe_5	36
4. 2 Carrier density of Ta_2NiSe_5	37
4. 3 High temperature transport properties of Ta_2NiSe_5	38
4. 4 Optical conductivity of Ta_2NiSe_5	39
4. 5 Specific heat anomaly at T_c	40
4. 6 Discussion of the chapter.....	41
4. 7 Summary of the chapter.....	42
Chapter 5 Electronic phase diagram of Ta_2NiSe_5	45
5. 1 Activation energy of sulfur substituted Ta_2NiSe_5	46
5. 2 T_c of chemical substituted Ta_2NiSe_5	48
5. 3 Pressure effect of pure, sulfur and tellurium substituted Ta_2NiSe_5	50
5. 4 Discussion of the chapter.....	52
5. 5 Summary of the chapter.....	52
Chapter 6 Superconductivity in $\text{Ta}_2\text{Pd}_x\text{S}_5$	55
6. 1 The crystal and the electronic structure of $\text{Ta}_2\text{Pd}_x\text{S}_5$	56

6. 2 Superconducting transition of $\text{Ta}_2\text{Pd}_x\text{S}_5$	56
6. 3 H_{c2} beyond the Pauli limit	58
6. 4 Discussion of the chapter.....	59
6. 5 Summary of the chapter.....	61
Chapter 7 Discussion	63
7. 1 Is Ta_2NiSe_5 an excitonic insulator?.....	63
7. 1. 1 Gap opening below T_c	63
7. 1. 2 The evidence of exciton condensation.....	64
7. 1. 3 The relevant energy scale of Ta_2NiSe_5	65
7. 1. 4 The electronic phase diagram	66
7. 1. 5 Supporting evidences of the excitonic insulator transition.....	68
7. 2 Uniqueness of Ta_2NiSe_5 as an excitonic insulator	71
7. 3 Future perspectives	74
Chapter 8 Summary	76
Appendix	79
Acknowledgement	83
Bibliography	84

Chapter 1 Introduction

Strong electron correlation driven phases are among the most intriguing phenomena in condensed matter physics. The history of strongly correlated systems has begun in the early days of the 20th century. The first major discovery is the unexpected insulating ground state realized in some $3d$ transition metal oxides. Band theory, kicked off by F. Bloch, gives the energy dispersion of electron as a function of momentum in the periodic lattice potential. It was pointed out that the valence bands and conduction bands are separated by a finite energy gap in semiconductors and insulators while the bands are not fully occupied in metals. This well explains the physical properties of metals and insulators, such as temperature dependence of electronic resistivity, optical absorption and magnetic susceptibility. However, E. J. W. Verway and J. H. de Bore discovered that the band theory cannot explain the insulating behavior of some $3d$ transition metal oxides such as NiO and CoO which were predicted to be metallic (Ni^{2+} : $[\text{Ar}] 3d^8$ and Co^{2+} : $[\text{Ar}] 3d^7$ systems) [1]. In order to explain the insulating behavior of those materials, N. F. Mott and J. Hubbard attributed to electron-electron correlation which can be emphasized in the $3d$ orbitals [2]. It is discussed that the electrons in such transition metal oxides feel strong onsite Coulomb interaction U since such orbitals are highly localized. If the electron-electron Coulomb interaction is sufficiently large compared with transfer integral t (or band width W), finite activation energy is required to move electrons and therefore some $3d$ transition metal oxides become insulators even the orbitals are only partially occupied. In strongly correlated materials, charge, spin, orbital and lattice degree of freedom are competing and entangled each other which may result in an exotic electronic phase. Due to such complex and competing interactions, the phase transitions are easily tuned by external field such as chemical doping, pressure effect and magnetic field. Nowadays, varieties of phase transitions have become one of the most intriguing fields in the strongly correlated systems since those give rise to drastic physical response as represented by high- T_c superconductivity in copper oxides [3,4] and colossal-magnetoresistance in manganese oxides as shown in Fig. 1-1 [5].

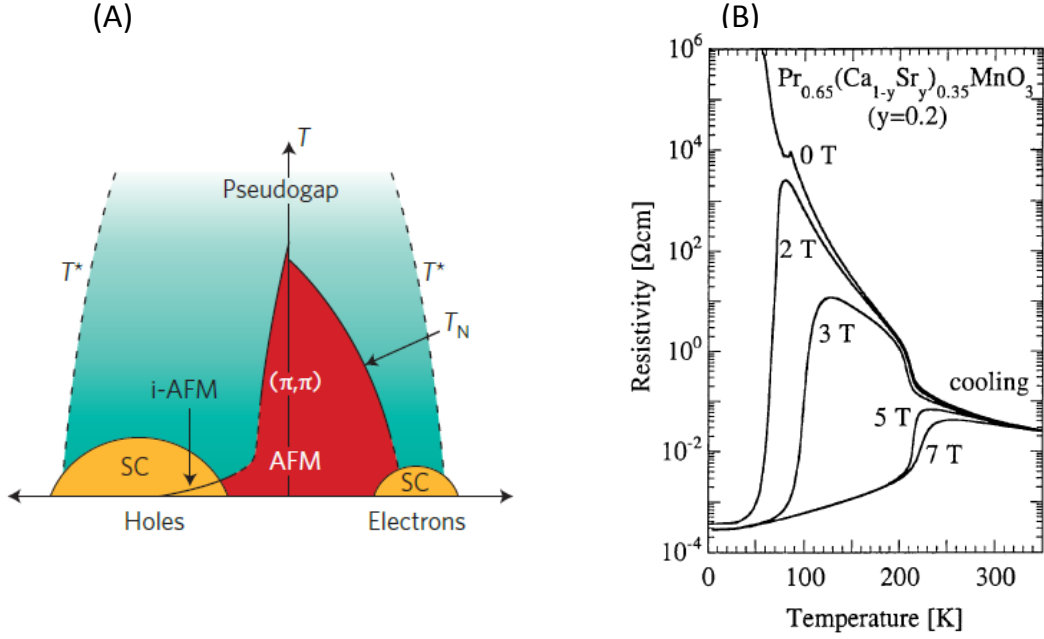


Figure 1-1: (A) Schematic electronic phase diagram of high- T_c cuprate as a function of carrier dopings (right: electron doping and left: hole doping) [4]. Anti-ferromagnetic order is suppressed and superconducting phase appears in both electron and hole dopings. (B) Electronic resistivity of a manganese oxide as a function of temperature [5]. Colossal magnetoresistance was observed under magnetic field.

While electron-electron interaction has been mainly focused in the strongly correlated systems, new exotic electronic phases have also theoretically been expected to manifest itself in the strong electron-hole coupling limit. One such exotic phase is an excitonic insulator. The presence of excitonic insulator transition was first suggested by N. F. Mott in semi-metallic systems with a small band overlap in 1961 [6]. The theoretical studies have further been developed by R. S. Knox [7], W. Kohn [8], B. I. Halperin and T. M. Rice [9], and excitonic insulator is now discussed to manifest itself in the semi-metal/semiconductor boundary, i.e. zero gap systems. It is discussed that excitonic insulator is originated from exciton condensation which can be described in analogy with the BCS theory of superconductivity [10]. The possibility of BCS-BEC crossover has also pointed out in the recent theoretical studies [10,11]. However, despite such intriguing characters, the experimental studies of excitonic insulator candidates are numbered and the presence of excitonic insulator has yet been identified. In this thesis, we report the transport, optical and thermodynamic properties of newly discovered excitonic insulator candidate Ta_2NiSe_5 . We show that a clear gap opens in the both

conduction and valence bands below T_c and large exciton binding energy is realized in Ta_2NiSe_5 , which can give rise to an excitonic insulator transition. The electronic phase diagram of Ta_2NiSe_5 was also investigated by tuning the magnitude of band gap, and we show that the obtained experimental results are consistent with theoretical predictions of excitonic insulator.

This thesis is organized as follows. First, we introduce the basic mechanism of excitonic insulator transition and old candidate materials studied so far, $\text{TmSe}_{0.45}\text{Te}_{0.55}$ and $1T\text{-TiSe}_2$. The remaining issues of those old candidate materials are also discussed. We then introduce the crystal and the band structure of newly discovered excitonic insulator candidate Ta_2NiSe_5 and show that it can be an ideal playground for the excitonic insulator studies in the **chapter 1**. In **chapter 2**, the objective of the study is mentioned. In order to establish the excitonic insulator state in Ta_2NiSe_5 , we have identified the magnitude of gap in the conduction and valence bands, respectively, and investigated the electronic phase diagram of Ta_2NiSe_5 by tuning the magnitude of band gap. In **chapter 3**, we present the experimental methods of sample preparation, characterization and physical properties measurements. In **chapter 4**, we present the experimental results of transport, optical and thermodynamic properties of Ta_2NiSe_5 . The gap formation and large entropy change associated with electron-hole hybridization can be identified in Ta_2NiSe_5 . In **chapter 5**, we report the electronic phase diagram of Ta_2NiSe_5 . The band gap of Ta_2NiSe_5 is tuned by sulfur (tellurium) substitution and pressure effect, respectively. We show that the obtained electronic phase diagram is consistent with the theoretical predictions. In **chapter 6**, we show the physical properties of $\text{Ta}_2\text{Pd}_x\text{S}_5$. Although the crystal structure of $\text{Ta}_2\text{Pd}_x\text{S}_5$ is different from that of Ta_2NiSe_5 , the electronic structure is similar. We discovered that new superconducting phase in $\text{Ta}_2\text{Pd}_x\text{S}_5$ and high upper critical field (H_{c2}) is realized. In **chapter 7**, we present the panoramic discussion of our study. We will compare the magnitude of exciton binding energy of Ta_2NiSe_5 with well-studied semiconductors such as ZnO and discuss why large exciton binding energy is realized in Ta_2NiSe_5 . Finally, taking the experimental data and discussion into account, we summarize our study which is given in **chapter 8**.

1. 1 What is an excitonic insulator?

Excitonic insulator is an electronic phase theoretically predicted to manifest itself by band hybridization between conduction and valence bands associated with exciton condensation [6-9]. Exciton is the quasi-particle composed of electron and hole and it can be observed in many semiconductors and insulators, including salts, oxides and III-V semiconductors [12]. Here we show the schematic band structure of an indirect gap semiconductor in Fig. 1-2 (A). In the semiconductor, conduction and valence bands are separated by finite band gap E_G . The energy level of exciton is slightly stabilized than the conduction band due to the Coulomb interaction between electron in conduction and hole in the valence band. However, in most of semiconductors, the magnitude of exciton binding energy E_B is smaller than the band gap E_G , and the energy level of exciton is higher than that of valence band. Therefore, exciton has finite life time and no phase transitions are expected even at 0 K due to exciton recombination. However, in a narrow gap semiconductor and a semi-metal with a small band overlap, the electron-hole interaction is only weakly screened due to the low carrier density and the exciton binding energy E_B may become comparable to the magnitude of band gap E_G . It is discussed that the original ground state (semiconducting or semi-metallic state) become unstable against exciton formation once exciton binding energy E_B exceeds the magnitude of band gap E_G , and system undergoes an excitonic insulator transition at T_c [8,9]. Fig. 1-2 (B) shows the schematic picture of excitonic insulator transition in the momentum space. Below T_c , excitonic gap Δ opens in both conduction and valence bands and new bands φ_a' and φ_b' are formed. It is discussed by W. Kohn that the new bands, φ_a' and φ_b' , can be described by the linear combination of Bloch wave function of original bands φ_a and φ_b , respectively [8]. In general, excitonic insulator transition is accompanied by a finite- \mathbf{q} lattice distortion with new periodicity $2\pi/|\mathbf{q}|$ and form excitonic gap Δ [8,9]. Here \mathbf{q} is the wave vector connecting conduction band minimum and valence band maximum which is illustrated in Fig. 1-2 (A). The finite- \mathbf{q} lattice distortion enlarges the lattice constant of materials and therefore size of the 1st Brillouin zone shrinks, and the original X point (π/a) becomes Γ point ($2\pi/2a$) of the 2nd Brillouin zone below T_c . The backfolded bands appear at Γ point and therefore the system becomes direct gap system which can hybridize conduction and valence bands each other.

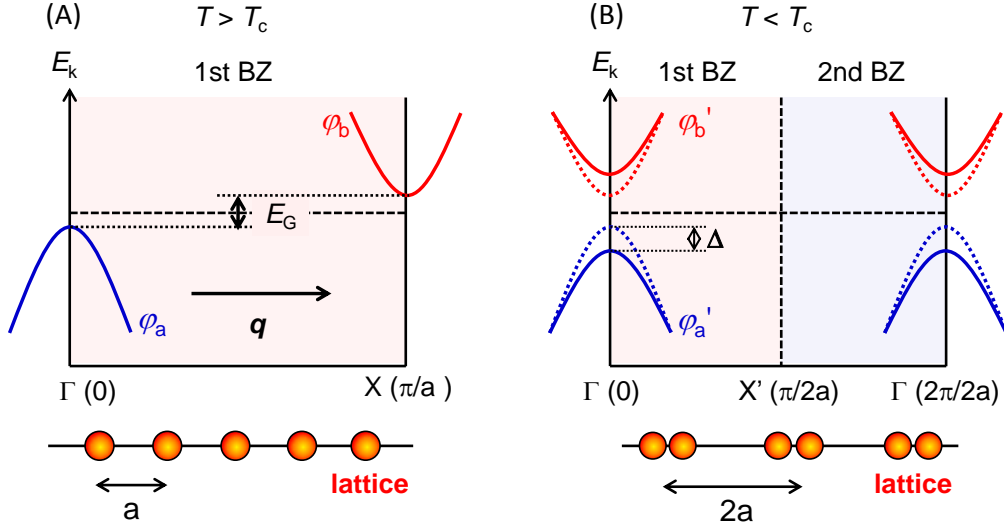


Figure 1-2: Schematic picture of excitonic gap formation in an indirect gap semiconductor. (A) The band and lattice structure of the indirect gap semiconductor above and (B) below T_c . The transition is accompanied by a finite- q lattice distortion associated with wave vector q ($q = k_X - k_\Gamma$), and new backfolded bands appear at Γ point below T_c . Excitonic gap Δ is expected to be formed in the both conduction and valence band. The φ_a and φ_b denote the Bloch functions of valence and conduction and the φ'_a and φ'_b can be expressed by the linear combination of original Bloch functions [8].

Within the excitonic insulator scenario, the exciton condensation can be described in analogy with the Bardeen-Cooper-Schrieffer (BCS) theory of superconductivity, however, the physical properties of excitonic insulator is highly different from that of superconductors [10]. While Meissner effect and zero resistance are the characteristic phenomena of superconductivity, electronic conductivity of excitonic insulator has been discussed to be suppressed below T_c since charge-neutral particle, exciton, does not contribute to electronic conductivity. Fig. 1-3 shows the theoretical prediction of renormalized electronic conductivity and effective carrier density below T_c which are proposed by J. Zittartz [13] and D. Jerome et al [14]. According to J. Zittartz, temperature dependence of electronic conductivity $\sigma(t)$ can be described by the following equation,

$$\frac{\sigma(t)}{\sigma_0} = 1 - A(1-t) \quad (1-1)$$

where σ_0 is the electronic conductivity at T_c , A is the substance-specific constant and t is the renormalized temperature T/T_c , respectively. We note that the electronic conductivity

does not contain Boltzmann term. If the exciton is in a spin-singlet state, excitonic insulator is considered to be a non-magnetic insulator. Therefore it is difficult to distinguish between the other insulating electronic ground state as represented by charge-density-wave (CDW) which can be widely observed in low dimensional materials, such as transition metal dichalcogenides [15-17].

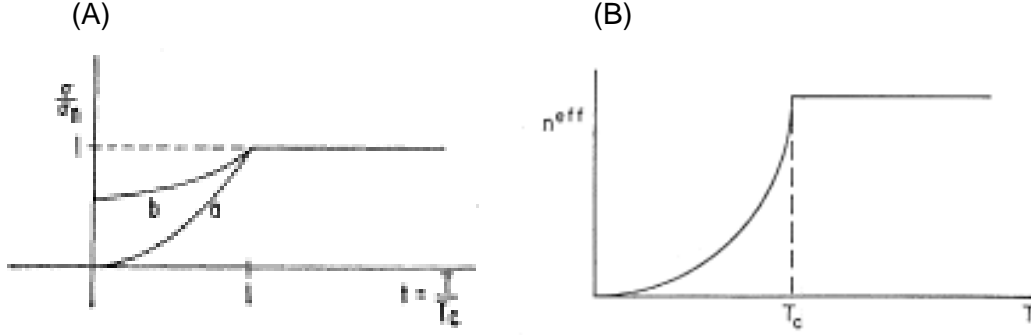


Figure 1-3: (A) The theoretically predicted electronic conductivity $\sigma(t)/\sigma_0$ of excitonic insulator state as a function of renormalized temperature t ($t = T/T_c$). The curves a and b denote the clean and dirty excitonic insulators, respectively [13]. (B) The theoretically calculated effective carrier density of excitonic insulator [14]. Both electronic conductivity and effective carrier density is discovered to be suppressed since charge-neutral particle, exciton, does not contribute to electronic conductivity.

One of the key predictions of theoretical framework describing the excitonic insulator phase is the characteristic dependence of the transition temperature T_c on the strength of the electron-hole Coulomb interaction, which can ultimately be controlled by tuning magnitude of band gap E_G [9,14]. In Fig. 1-4 we show the generally predicted electronic phase diagram. The excitonic insulator state is theoretically predicted to be the most stable at semi-metal/semiconductor boundary, and increased and decreased E_G suppress T_c of the phase transitions. For negative E_G (band overlap), the increased carrier density screens and reduces the effective Coulomb interaction between electron and hole. The exciton binding energy E_B is therefore suppressed and consequently T_c . This is in strong contrast to a simple hybridization gap, which is expected to persist for large band overlap and finite electron density at the Fermi energy. For positive E_G (the semiconducting phase), exciton formation and condensation becomes thermodynamically unstable against the semiconducting ground state and T_c is suppressed very quickly. Theoretically, the transition from semimetal-to-excitonic insulator can be described in analogy with BCS theory of superconductivity while

Bose-Einstein condensation (BEC) of exciton is predicted in the semiconductor region [10,11]. While BCS-BEC crossover have been studied in cold atom, which requires ultra-low temperature [17], T_c of BEC transition in excitonic insulator can be much higher since the electron and hole masses are approximately 1000 times smaller than that of atomic masses. Therefore, excitonic insulator can be a solid-state platform to explore high temperature BCS-BEC crossover. Furthermore, presence of a high- T_c superconducting phase has been theoretically discussed in proximity to an excitonic insulator. It is discussed by P. Bhattacharyya et al. that system may transform into a superconducting state in the semi-metallic region by applying pressure [18].

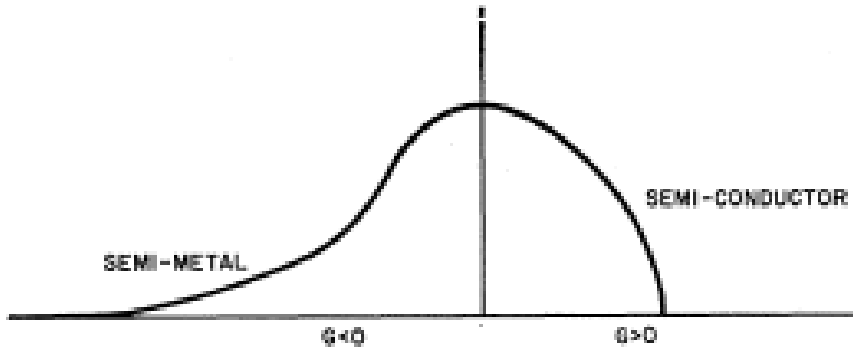


Figure 1-4: Theoretically predicted phase diagram of excitonic insulator as a function of band gap E_G . It is discussed that the exciton condensation can be described in the analogy of BCS theory in the semi-metallic side while Bose-Einstein condensation of exciton is expected in the semiconductor side of the phase diagram [14].

1. 2 Excitonic insulator candidate materials

Despite such intriguing features and expectations, only a handful of candidates have been reported to date for an excitonic insulator. In this section, we introduce the well-studied candidate materials $1T$ -TiSe₂ [19,20] and TmSe_{0.45}Te_{0.55} [21-23]. Here we show the phase transition of $1T$ -TiSe₂ and TmSe_{0.45}Te_{0.55}, and discuss why excitonic insulator states have been invoked in those systems at first. Second, the remaining issues of those materials are discussed and we propose that direct gap semiconductors or semi-metals could be the ideal playground for excitonic insulator studies.

1. 2. 1 TmSe_{0.45}Te_{0.55}

One of the famous excitonic insulator candidates are the TmSe_{0.45}Te_{0.55} which crystallizes in the NaCl-type crystal structure (Space group: $Fm\bar{3}m$, No. 225) as shown in Fig. 1-5 (A). The TmSe-TmTe solid solution systems are unique among the rare earth monochalcogenides which shows mixed valence state [24]. The band calculation indicates that the valence band of Tm Ch (Ch = sulfur, selenium and tellurium) are composed of Tm $4f$ orbitals while Tm $5d$ ($5s$) orbitals dominate conduction band, respectively. Although $4f$ orbitals of Tm ion are not fully occupied, $4f$ electrons do not contribute to electronic conductivity since the orbitals are highly localized. The band gap of Tm monochalcogenides are determined by the separation in energy of the $4f^{12}(5d6s)^1$ and $4f^{13}(5d6s)^0$ configuration as shown in Fig. 1-5 (B) [25]. In TmTe, the energy level of $4f^{13}$ state is expected to be slightly lower than that of $5d$ (t_{2g}) orbitals and therefore TmTe has 13 $4f$ -electrons, i.e. Tm $5d$ orbitals are empty. Therefore finite activation energy which corresponds to the energy difference between Tm $5d$ and $4f^{13}$ state is required for electronic conductivity. As isovalent (selenium) substitution increases, the energy level of conduction band is lowered due to chemical pressure associated with smaller ionic radius of selenium, and the system is driven into metallic state when the energy level of $4f^{12}(5d6s)^1$ and $4f^{13}(5d6s)^0$ configuration become the same. Indeed, the electronic resistivity measurements show that TmTe is a semiconductor with a band gap of ~ 0.3 eV while TmSe and TmS are metallic, respectively [26-29]. The electronic and spin configuration of Tm monochalcogenide is furthermore evidenced by the magnetic susceptibility. [30]. In order to realize a narrow gap semiconductor in the system, P. Bucher et al. synthesized TmSe_{0.45}Te_{0.55} with energy gap E_G of ~ 0.15 eV which does not show any phase transition under ambient pressure [29].

The pressure induced semiconductor-to-insulator transition is the key experimental evidences which suggest the presence of excitonic insulator state in the system [21-23]. Since TmSe_{0.45}Te_{0.55} does not show any phase transitions under ambient pressure, TmSe_{0.45}Te_{0.55} is considered to be located at outside of the characteristic phase diagram within the excitonic insulator scenario. Pressure effect should drive the system to be more metallic and dome-like electronic phase diagram of excitonic insulator is expected as shown in the Fig. 1-4. Fig. 1-5 (C) shows the electronic resistivity of TmSe_{0.45}Te_{0.55} as a function of pressure at several temperature ranges [21]. It is discovered that the system becomes more insulating at around 0.5 GPa and then the phase transition is suppressed by further applying pressure. The semiconductor-to-insulator transition is furthermore confirmed by Hall measurement

[22]. Decreased carrier density is clearly observed at the corresponding pressure range. An excitonic insulator transition is discussed in the system since the T_c of the phase transition is found to be sensitive to the magnitude of pressure and therefore sensitive to the band gap E_G which is consistent with excitonic insulator scenario [23].

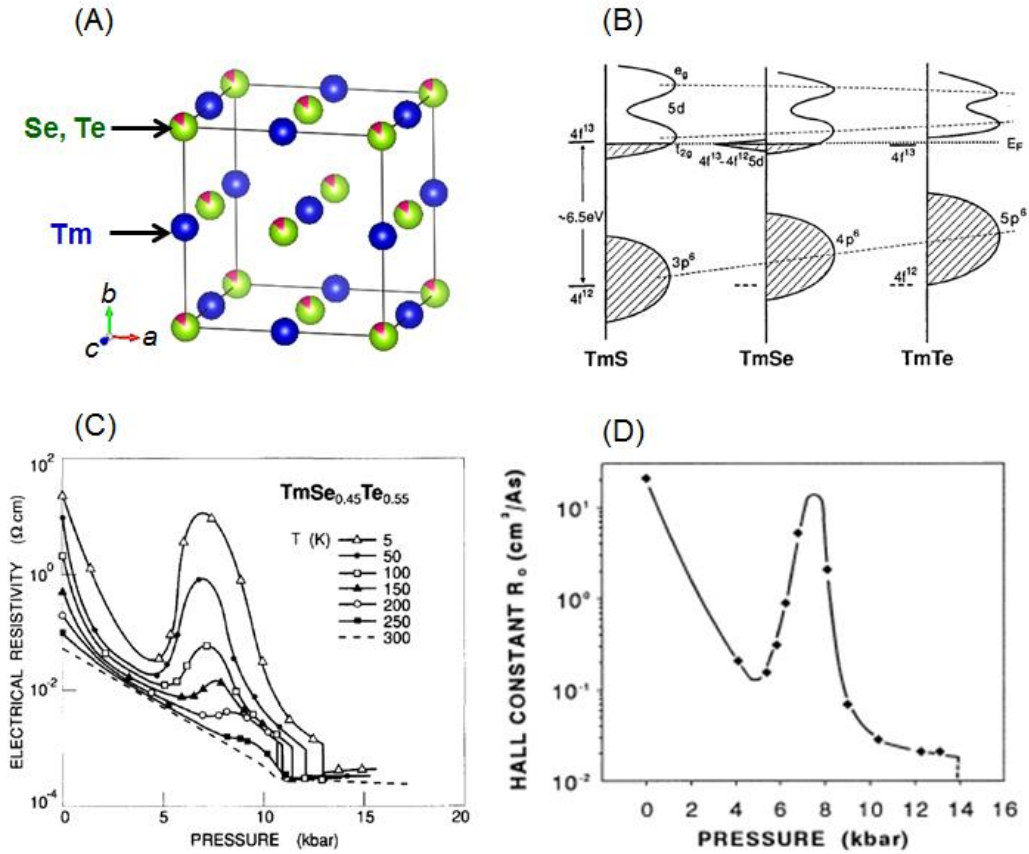


Figure 1-5: (A) The room temperature crystal structure and (B) the calculated electronic structure of $\text{TmSe}_{0.45}\text{Te}_{0.55}$. (C) Electronic resistivity of $\text{TmSe}_{0.45}\text{Te}_{0.55}$ as a function of pressure taken at 5 – 250 K (solid line). The dashed line denotes the data points taken at 300 K [21]. (D) Hall constant of $\text{TmSe}_{0.45}\text{Te}_{0.55}$ as a function of pressure taken at 4.2 K. A significant decrease of effective carrier density can be identified at corresponding pressure [22].

1. 2. 2 1*T*-TiSe₂

1*T*-TiSe₂ is the second candidate material of excitonic insulator [19,20] which is expected to manifest itself in the semi-metallic region. The room temperature crystal structure is illustrated in Fig. 1-6 (A) [31]. It was found to crystallize in the 1*T*-type (Cd(OH)₂-type) structure (Space group $P\bar{3}m1$, No. 164). Titanium atoms are octahedrally coordinated by selenium atoms and each TiSe₂ layer is loosely stacked by van der Waals interaction. The reported band calculation indicates that the Ti 3*d* (*t*_{2g}) orbitals dominate the conduction bands while valence bands are composed of Se 4*p* orbitals in this system, respectively [32]. It is pointed out that the system is a compensated metal since there is a finite overlap between conduction and valence band. Fig. 1-6 (B) shows the electronic resistivity of 1*T*-TiSe₂ [33]. As expected from the band calculation, 1*T*-TiSe₂ is discovered to be a semi-metal in the high temperature phase and it undergoes a phase transition at 202 K accompanied by a periodic lattice distortion under ambient pressure [34]. Decreased carrier density can be identified from Hall measurement which gives approximately $n \sim 3 \times 10^{20} \text{ cm}^{-3}$ at 300 K and $n \sim 6 \times 10^{19} \text{ cm}^{-3}$ at 100 K, respectively, suggesting a gap formation at Fermi level in the low temperature phase [35]. A CDW is first proposed to explain the origin of phase transition since the transition is accompanied by $2 \times 2 \times 2$ periodic lattice distortion which is consistent with Fermi surface nesting vector between Γ and L point [32,34].

Recently and however, the possibility of excitonic insulator state was proposed according to the ARPES studies [19,20]. Fig. 1-6 (C) shows the valence band and part of conduction band of 1*T*-TiSe₂ taken by using ARPES technique below and above T_c . It is clearly seen that the energy level of valence band is lowered below T_c (gray dashed line), suggesting a gap formation which is consistent with the transport data. Excitonic insulator scenario is proposed in the system since strong spectral weight transfer is observed in the low temperature phase. At Γ point, the energy level of the topmost Se 4*p* bands are approximately 100 meV stabilized accompanied by a large decrease of the spectral weight. Instead, a very clear backfolded valence band appears at M point. The spectral weight transfer is found to be approximately 35 % in 1*T*-TiSe₂. The obtained experimental results exclude the possibility of conventional CDW to explain the phase transition of 1*T*-TiSe₂ since only a few percent of spectral weight transfer is expected in conventional CDW scenario which is originated from Fermi surface nestingⁱ [36].

ⁱ It is discussed by J. Voit et al. that magnitude of the spectral transfer in CDW transition depend on the ratio Δ/W , where Δ is the half gap and W is the band width [36]. In 1*T*-TiSe₂, Δ and W is reported to be $\Delta \sim 100 \text{ meV}$ and $W \sim 3 \text{ eV}$, giving $\Delta/W \sim 3 \%$ which is much smaller than experimental data.

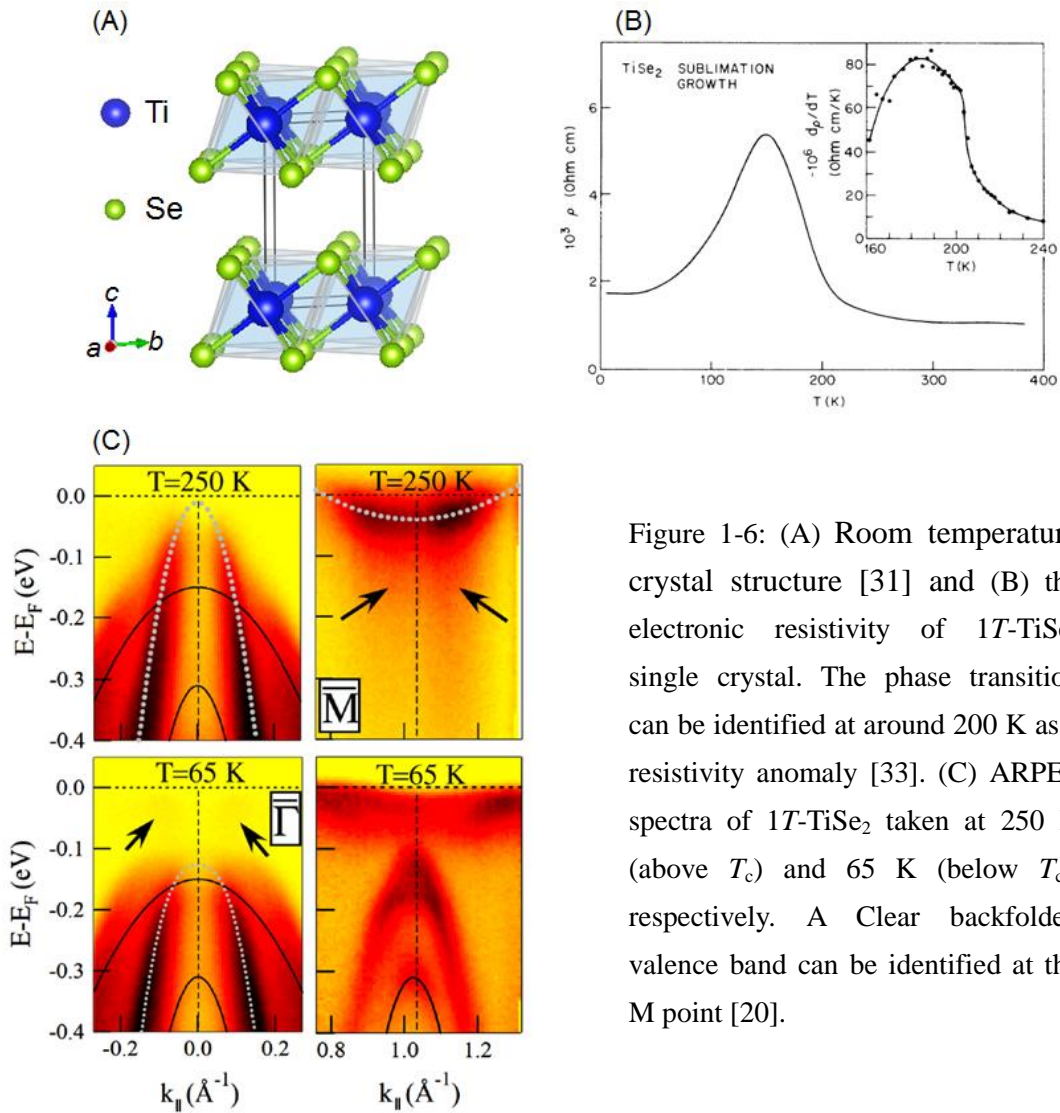


Figure 1-6: (A) Room temperature crystal structure [31] and (B) the electronic resistivity of 1T-TiSe₂ single crystal. The phase transition can be identified at around 200 K as a resistivity anomaly [33]. (C) ARPES spectra of 1T-TiSe₂ taken at 250 K (above T_c) and 65 K (below T_c), respectively. A Clear backfolded valence band can be identified at the M point [20].

1. 2. 3 Issues in the existing excitonic insulator candidates

The two candidate materials have been studied for a long time, however, these still remain issues to identify the presence of excitonic insulator state, yet. Both of the two materials are known as indirect gap systems and the phase transition is accompanied by a finite- q lattice distortion within the excitonic insulator scenario [8,32]. This makes difficult to establish an excitonic insulator state since the physical properties are similar to that of a CDW state which is hardly to be distinguished. Furthermore, the strong lattice distortion and magnetic momentum obscure the intrinsic physical responses of these phase transitions. In this section, the remaining issues and counter arguments which explain the origin of the phase transition of two candidate materials,

$\text{TmSe}_{0.45}\text{Te}_{0.55}$ and $1T\text{-TiSe}_2$, are discussed.

$\text{TmSe}_{0.45}\text{Te}_{0.55}$: Thermodynamic property is a key experimental evidence in order to identify excitonic insulator state since exciton condensation should make a significant change in the electronic heat capacity. B. Bucher et al. measured AC heat capacity of $\text{TmSe}_{0.45}\text{Te}_{0.55}$ under pressure, however, no heat capacity anomaly is identified at T_c [37]. Instead, the authors observed significant change of heat capacity contributed by lattice system. Fig. 1-7 (A) shows the AC heat capacity of $\text{TmSe}_{0.45}\text{Te}_{0.55}$ under pressure. At ambient pressure, the lattice heat capacity is well described by Debye function while the heat capacity is found to be linear as a function of temperature at around T_c under 0.6 GPa (pink solid line). It is discussed that the excitonic insulator transition in the indirect gap system requires a finite- q lattice distortion which results in significant change in the heat capacity contributed by lattice system. Therefore the lattice distortion hinders entropy change associated with the phase transition in the electronic system.

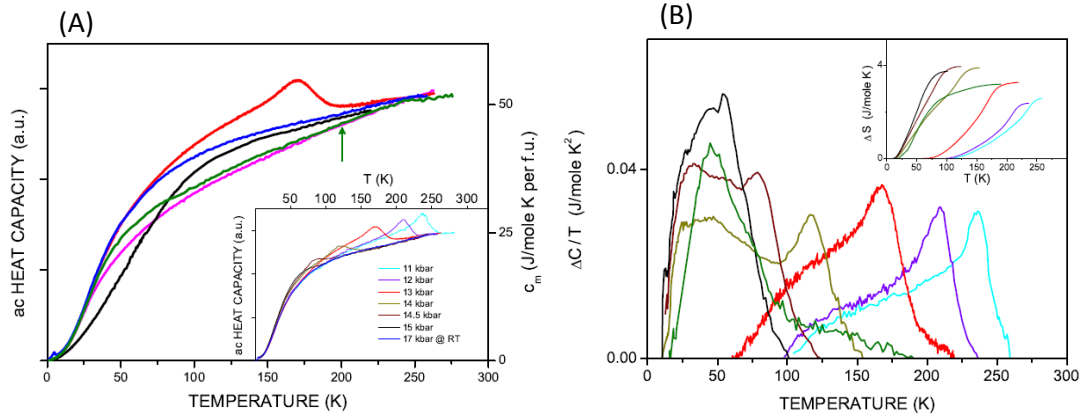


Figure 1-7: (A) AC heat capacity measurement of $\text{TmSe}_{0.45}\text{Te}_{0.55}$ under pressure and (B) estimated entropy change obtained by subtracting lattice contribution [37]. At around $P \sim 0.6$ GPa, the obtained heat capacity is flat while the heat capacity can be well described by Debye function under ambient pressure. The inset of (A) represents AC heat capacity of $\text{TmSe}_{0.45}\text{Te}_{0.55}$ in the pressure range of 1.1 GPa to 1.6 GPa. Clear heat capacity anomalies can be identified at which is discussed to be originated from change of spin configurations.

Spin degree of freedom of Tm ion is also found to play a significant role in the heat capacity signature of this system. At 1.1 ~ 1.6 GPa, clear anomalies can be identified in the heat capacity measurements. However, it was pointed out that the heat capacity anomalies do not originate from the exciton condensation, but change of electron and spin configuration of Tm ion. It is discussed that the system is driven into semi-metallic state by pressure effect and Tm ion become $4f^{13}(5d6s)^0$ to the $4f^{12}(5d6s)^1$ configurations. This results in entropy change of $\Delta S = 3.98 \text{ J}/(\text{mol K})^{\text{ii}}$, showing good agreement with experimental data as shown in Fig. 1-7 (B). This is in strong contrast to the ideal excitonic insulator transition where the thermodynamics of the phase transition is dominated by large entropy changes in the charge sector only with the necessary accompanying lattice deformation being a negligible secondary effect through electron-phonon coupling.

1T-TiSe₂: 1T-TiSe₂ is also an indirect gap system and the phase transition is accompanied by a finite- q lattice distortion [32,34]. The crystal structure of 1T-TiSe₂ below and above T_c is illustrated in Fig. 1-8 (A) [31]. The crystal field of TiSe₆ octahedra (1T) becomes TiSe₆ trigonal prism (2H) below T_c in the system. Therefore the crystal deformation complicates the electronic structure and obscures the exact evaluation of gap opening associated with the phase transition. For example, in 1T-TiSe₂, the energy level of both conduction and valence bands are found to be lowered below T_c by using ARPES technique [38]. It is in strong contrast to the excitonic insulator scenario which opens an excitonic gap in both conduction and valence band (see Fig. 1-2) [8]. Consequently, a band Jahn-Teller effect is proposed to explain the origin of phase transition in 1T-TiSe₂ [38,39]. Fig. 1-8 (C) shows the electronic structure below and above T_c within the band Jahn-Teller scenario. The energy levels of the two crystal field, octahedra and trigonal prism, have been discussed in 1T-TaS₂ and 2H-TaS₂ [39,40]. It is expected that while Ta 5d (t_{2g}) orbitals are most stable in TaS₆ octahedra while Ta $5d_z^2$ orbital become more stable in TaS₆ trigonal prism, and therefore electronic system can be stabilized within the band Jahn-Teller scenario (see Fig. 1-8 (C)).

ⁱⁱ The spin entropies for the Tm: $4f^{12}(5d6s)^1$ and Tm: $4f^{13}(5d6s)^0$ configuration can be calculated to be $S_{\text{spin}}/k_B = \ln(2J + 1) = 2.08$ ($J = 7/2$) and $S_{\text{spin}}/k_B = \ln(2J + 1) = 2.56$ ($J = 6$), respectively. This gives entropy change of the spin sector to be $\Delta S = 0.48R = 3.98 \text{ J}/(\text{mol K})$, giving good agreement with experimental results as summarized in the inset of Fig. 1-9 (B).

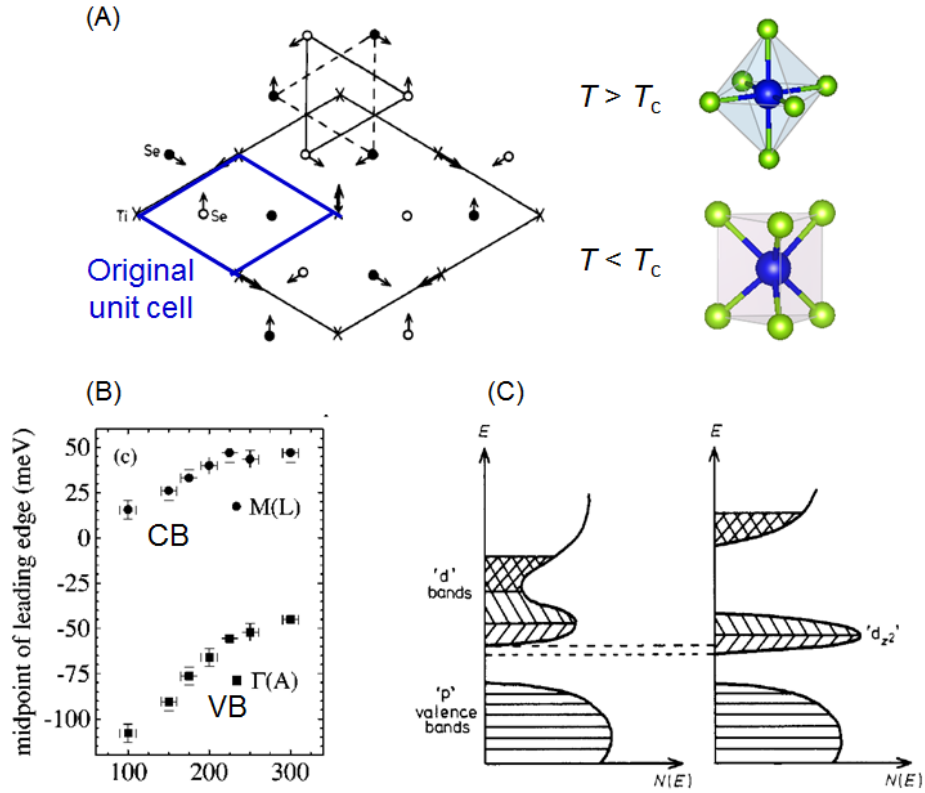


Figure 1-8: (A) The crystal structure of 1T-TiSe₂ above and below T_c . In the high temperature phase, the crystal field of TiSe₆ is octahedra while it becomes TiSe₆ trigonal prism below T_c [39]. (B) The minimum point of conduction and the maximum point of valence bands as a function of temperature measured by using ARPES technique [38]. Both of valence and conduction bands are stabilized as temperature is lowered. (C) Schematic picture of energy level of $3d$ (t_{2g}) in the octahedral coordination and $3d_z^2$ in the trigonal prism [39,40]. The energy level of TiSe₆ trigonal prism is expected to be more stable within the band Jahn-Teller scenario.

Both of TmSe_{0.45}Te_{0.55} and 1T-TiSe₂ are the indirect gap systems and the phase transition is accompanied by a finite- q lattice distortion. This obscures the intrinsic physical quantities of an excitonic insulator since such strong lattice distortion modifies the electronic structure of materials beyond the naive argument of electron-hole hybridization. In order to evidence the presence of excitonic insulator state, it is required to avoid such strong lattice distortion. Therefore, a narrow gap semiconductor or a semi-metal with a direct gap band structure ($q = 0$) is highly demanded for the excitonic insulator studies.

1. 3 A new excitonic insulator candidate Ta_2NiSe_5

Recently, Ta_2NiSe_5 emerged as a prime candidate material of excitonic insulator. In this section, we introduce the crystal and the band structure of Ta_2NiSe_5 and discuss that it can be an ideal playground of excitonic insulator research at first. Second, we introduce the previous X-ray Photoemission Spectroscopy (XPS) and Angle Resolved Photoemission Spectroscopy (ARPES) studies which suggest an excitonic gap formation in the Fermi level of Ta_2NiSe_5 .

1. 3. 1 The crystal and the band structures

The crystal and the calculated band structure of Ta_2NiSe_5 are illustrated in Fig. 1-9. In the high temperature phase, Ta_2NiSe_5 crystallizes in a layered structure with an orthorhombic unit cell. Each Ta_2NiSe_5 layer is loosely stacked by van der Waals interaction, and is composed of quasi-one dimensional chains of corner-shared NiSe_4 tetrahedra and edge-shared TaSe_6 octahedra (see Fig. 1-9 (A) and (B)) [41,42]. The band calculation indicates a finite direct gap at the Γ point ($\mathbf{q} = 0$) in Ta_2NiSe_5 [43]. The valence band is mainly composed by Ni $3d$ orbitals with Se $4p$ admixture while Ta $5d$ orbitals dominate the conduction band, indicating that Ta $5d$ orbitals are empty while Ni $3d$ and Se $4p$ orbitals are fully occupied. This leads to the exceptional situation among excitonic insulator candidates in which the carriers of the valence and conduction bands both exist at the Γ point in momentum space while being spatially separated in real space, realising a direct gap semiconductor. Crucial for this is that in the high temperature phase, the valence and conduction band belong to the different irreducible representations of the crystal structure [43]. Therefore the formation of a single particle hybridization gap is forbidden by the crystal symmetry and each valence and conduction bands have strong one dimensional character. Due to this, a small direct gap semiconductor can be realised in the system above the transition temperature T_c which can be an ideal situation for excitonic insulator phase transition.

The electronic resistivity of Ta_2NiSe_5 is approximately $\sim 10^{-3} \Omega\text{cm}$ above T_c and shows semiconductor-like temperature dependence as shown in Fig. 1-10 (A). It is discovered that Ta_2NiSe_5 undergoes a semiconductor-to-insulator transition at 328 K without finite- \mathbf{q} structural distortion. Instead, the phase transition is accompanied by a small and uniform lattice distortion which lowers crystal symmetry from orthorhombic to the monoclinic unit cell [41,42]. The phase transition is evidenced by electronic resistivity and magnetic susceptibility measurements. The electronic resistivity is

significantly enhanced while clear suppression of magnetic susceptibility was reported, indicating that non-magnetic insulator is the ground state in Ta_2NiSe_5 below T_c (see Fig. 1-10) [42].

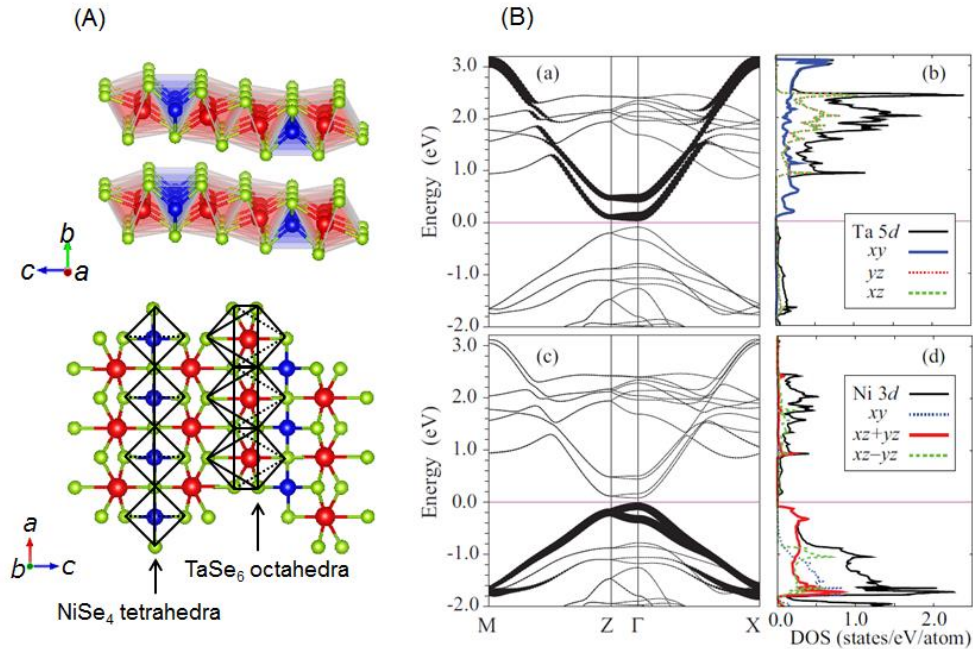


Figure 1-9: (A) Room temperature crystal structure of Ta_2NiSe_5 [41,42]. The Ta_2NiSe_5 layers are composed by corner shared NiSe_4 tetrahedra and edge shared TaSe_6 octahedra, respectively. (B) Calculated band structure of high temperature phase Ta_2NiSe_5 [43]. Valence band is composed by $\text{Ni } 3d$ and $\text{Se } 4p$ orbitals while $\text{Ta } 5d$ orbitals dominate conduction band. Both of conduction and valence band have quasi-one dimensional characters.

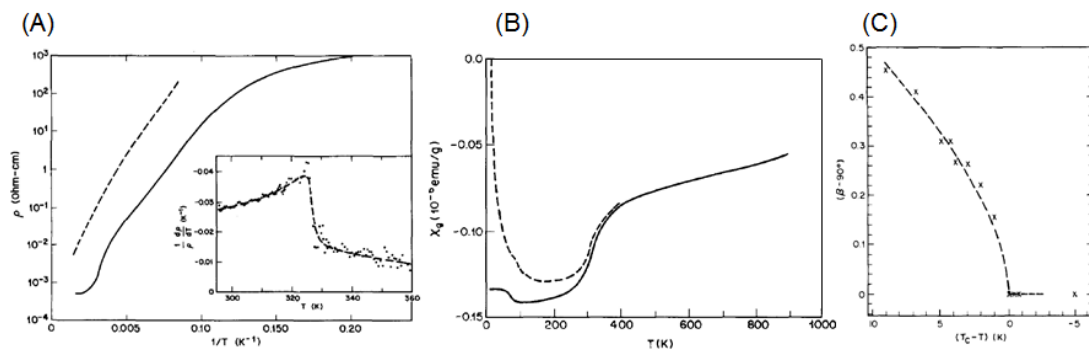


Figure 1-10: (A) Electronic resistivity (B) magnetic susceptibility and (C) the angle β as a function of temperature [42]. Clear anomaly can be identified at 328 K, indicating semiconductor-to-insulator transition. The phase transition is accompanied by small and uniform crystal deformation which lowers crystal symmetry from orthorhombic to monoclinic unit cell.

1. 3. 2 Proposal for an excitonic insulator state in Ta₂NiSe₅

The origin of phase transition in Ta₂NiSe₅ has not been interpreted for several decades, but recently, excitonic insulator transition was invoked by XPS and ARPES measurement [44]. XPS is a powerful method to measure the binding energy of core electron and identify the oxidation state of materials. Y. Wakisaka et al. discovered that the Ta 5*d* orbitals and Ni 3*d* (Se4*p*) orbitals are partially hybridized by using XPS technique [44]. Fig. 1-11 shows the Ni 2*p*_{3/2} core-level spectrum which was taken at 40 K and 300 K, i.e. below *T*_c. While the main sharp peak is clearly seen at -853 eV, the satellite peak also can be identified at around -861 eV. It is discussed that the presence of the satellite peak hallmarks the partially occupied Ni 3*d* orbitals. In fact, the obtained XPS spectrum is well described by the linear combination of *d*⁸, *d*⁹*L* and *d*¹⁰*L*² configurations where *L* denotes a hole in Se 4*p* orbitals, respectively, which suggests that the formal oxidation state of the system is Ta⁴⁺ and (NiSe₅)⁸⁻, respectively. According to the results, the conduction band and valence bands are only partially occupied and therefore the system is expected to be a metal or semi-metal. Ta₂NiSe₅ is, however, discovered to be a non-magnetic insulator below *T*_c according to the electronic resistivity and magnetic susceptibility measurements [42]. This unexpected valence state strongly implies spin-singlet formation between electron of Ta⁴⁺ and hole of Ni²⁺ in order to explain the non-magnetic insulator ground state in Ta₂NiSe₅ which is consistent with excitonic insulator scenario.

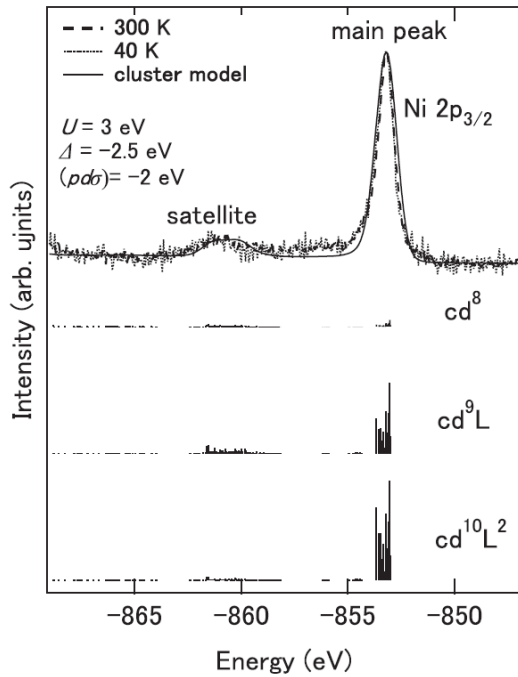


Figure 1-11: Ni 2*p*_{3/2} core-level spectra of Ta₂NiSe₅ taken by using XPS technique at 300 K (black broken line) and 40 K (black dashed line) [44]. The experimental data point can be reproduced by the linear combination of *cd*⁸, *cd*⁹*L* and *cd*¹⁰*L*² components which are obtained by using the NiSe₄ cluster calculation.

The ARPES, on the other hands, is a useful technique to observe the band structure (valence band) of Ta_2NiSe_5 experimentally. Fig. 1-12 shows the valence band of Ta_2NiSe_5 below and above T_c taken by using APRES technique with probing photon momentum along the X- Γ -X direction [11]. The black point is the obtained experimental data and the black solid line is the parabolic band fitted from the high energy points which are not related to the phase transition. It is readily seen that clear band gap opens in the valence band below T_c . Intriguingly, a very flat band below T_c can be identified at Γ point which is not expected from the band calculation. Carrier condensation is highly suggested by the flatness of valence band, and excitonic insulator state is thus invoked from the experimental data.

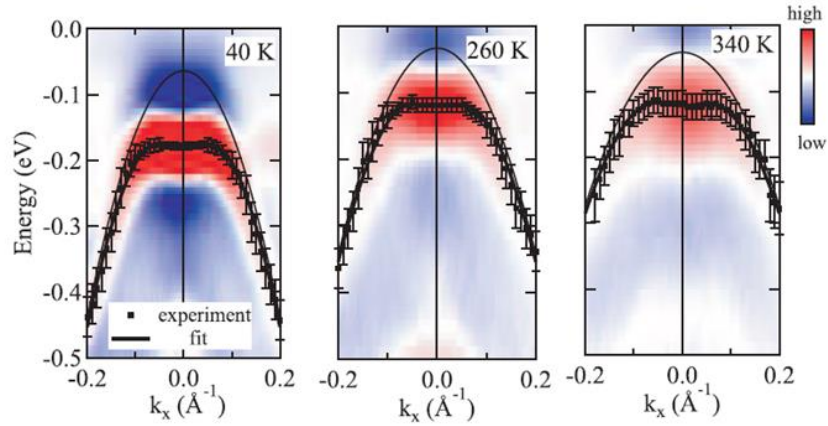


Figure 1-12: Valence band spectrum of Ta_2NiSe_5 in the various temperature range taken by using ARPES technique [11]. The photon is radiated along the X- Γ -X direction. The black points are the experimental data and black solid lines are the parabolic line fitted from high energy data point. It is clearly seen that finite gap opens in the valence band below T_c with band flattening.

Chapter 2 Objective

In this thesis, we aimed to elucidate the excitonic insulator phase in Ta_2NiSe_5 experimentally. As mentioned in chapter 1, Ta_2NiSe_5 is considered to be a narrow gap semiconductor with a direct gap band structure at Γ point ($q = 0$) and no finite- q lattice distortion has observed below T_c [41,42]. It is in strong contrast to the old excitonic insulator candidate materials, such as $1T\text{-TiSe}_2$ and $\text{TmSe}_{0.45}\text{Te}_{0.55}$, and therefore allows us to measure the physical properties of Ta_2NiSe_5 by ruling out the effects of lattice distortion [27,38]. In order to establish the excitonic insulator state, it is indispensable to identify the excitonic gap formation and the entropy change associated with exciton condensation. Furthermore, the characteristic phase diagram, shown in Fig. 1-4, should be a compelling experimental evidence of excitonic insulator. In an excitonic insulator, the phase transition is stabilized at around semi-metal/semiconductor boundary while increased and decreased band gap E_G suppress T_c [8,9,14].

2. 1 Basic physical properties of pure Ta_2NiSe_5

While Ta_2NiSe_5 emerged as a prime excitonic insulator candidate after the spectroscopic studies [11,44], the basic physical properties of pure Ta_2NiSe_5 are still unknown. In an excitonic insulator, excitonic gap associated with exciton condensation opens in both conduction and valence bands below T_c [8]. This should give rise to a significant change in the electronic heat capacity since the condensed carriers lose their entropy. While the gap formation and large entropy change are the generic features of an excitonic insulator, neither of them has been identified experimentally in Ta_2NiSe_5 . In order to address these issues and check the consistency with excitonic insulator scenario, we focused on basic physical properties of pure Ta_2NiSe_5 , especially transport, optical and thermodynamic properties.

Transport properties: Since Ta_2NiSe_5 is considered to be a narrow gap semiconductor, it is required to evaluate the magnitude of activation energy above T_c for the first step. In order to avoid the effect of pseudo-gap formation, discussed by K. Seki et al., transport properties including high temperature measurements are required.

Optical conductivity: Optical conductivity is one of the most powerful methods to identify the gap formation in Ta_2NiSe_5 below T_c . With combination of high temperature

transport and previous spectroscopic studies, we demonstrate that excitonic gap 2Δ manifest itself in Ta_2NiSe_5 below T_c .

Heat capacity measurement: The electronic heat capacity is obtained by subtracting lattice contribution which is described by Debye functions. The entropy change associated with the phase transition can be calculated by integrating electronic heat capacity C_{el}/T up to T_c .

2. 2 Electronic phase diagram in Ta_2NiSe_5

Electronic phase diagram is one of the key experimental evidences of excitonic insulating transition as well as transport, thermodynamic and optical properties [8,9,14]. As mentioned in the chapter 1, T_c of excitonic insulator strongly depends on the magnitude of band gap E_G . Since Ta_2NiSe_5 is reported to undergo a phase transition at 328 K, it is required to drive the system to be larger and smaller E_G , respectively [42]. Pressure effect is the simplest and cleanest method to drive the system into the semi-metallic state. We investigated T_c of Ta_2NiSe_5 as a function of pressure to draw the phase diagram of semi-metallic side. However, the phase diagram of semiconducting side cannot be achieved only by pressure effect. In order to drive the system into semiconductor state, we employed isovalent chemical doping. Isovalent chemical doping has two major effects which control the magnitude of band gap E_G ; **chemical pressure** and **band reconstruction**. As lattice constant is reduced by the chemical doping, the system is considered to be more metallic due to the increased orbital overlap, i.e. band width. The system is driven to be more insulating, on the other hands, if the lattice constant becomes larger. The effect of chemical pressure is emphasized when the substituted atoms are not responsible for the bands which are close to Fermi level. However, if the valence or conduction band is composed by the substituted atoms, the second effects become more significant. Here we discuss the isovalent chemical doping effect of sulfur (tellurium) and palladium.

S (Te) doping into Se site: As discussed by T. Kaneko et al [43]., band calculation indicates that the valence band of Ta_2NiSe_5 is composed of Ni $3d$ and Se $4p$ orbitals. With increased sulfur doping, the hybridization between Ni $3d$ and Se $4p$ (S $3p$) orbitals are weakened since the energy level of S $3p$ orbitals are lower than that of Se $4p$ orbitals. This eventually lowers the energy level of the valence band while the conduction band

is less affected, resulting in an overall enhancement of the energy gap compared to Ta_2NiSe_5 . Tellurium doping, on the other hand, pushes the system in the opposite direction. The stronger hybridization between Ni $3d$ and Te $5p$ orbitals leads to the valence bands being at higher energy which drives system to be more metallic.

While chemical pressure should drive the system to be more metallic in sulfur substituted Ta_2NiSe_5 , the effect of band reconstruction is considered to be more significant. The energy level of chalcogen p -orbitals have been discussed for a long time in the well-studied transition metal dichalcogenides. Fig. 2-1 shows the light absorption and measured band gap of $\text{Zr}(\text{Se}_{1-x}\text{S}_x)_2$ solid solutions as a function of sulfur content [45]. It is clearly seen that the band gap of ZrS_2 is larger than that of ZrSe_2 while chemical pressure should drive the system to the opposite direction.

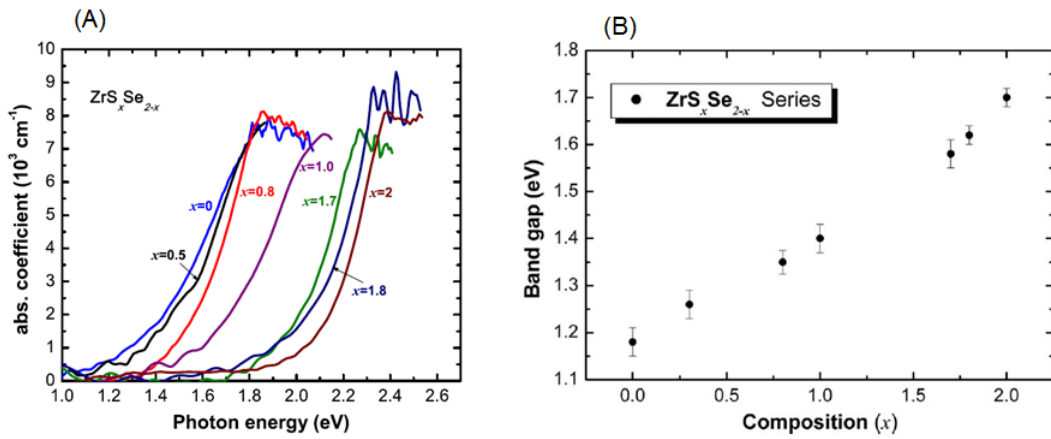
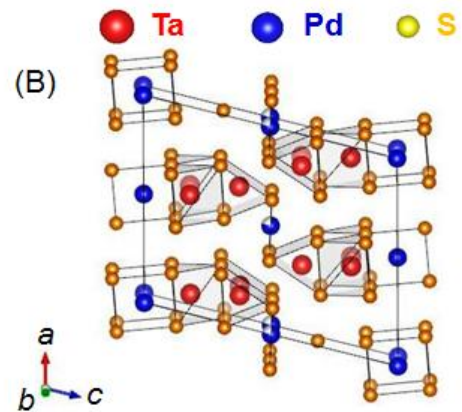
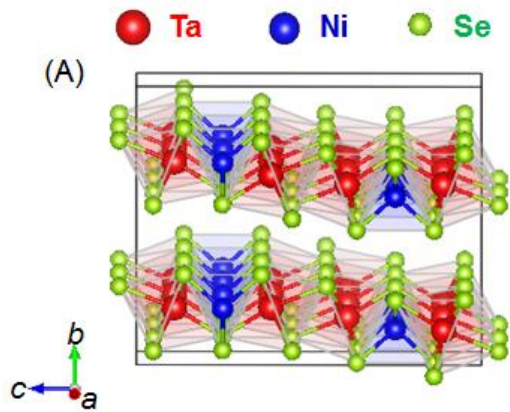


Figure 2-1: (A) Light absorption of $\text{ZrS}_x\text{Se}_{2-x}$ solid solution and (B) its corresponding band gap measured by the light absorption. The magnitude of band gap is found to be enhanced as sulfur content increases [45].

Pd doping into Ni site: Palladium substitution is considered to drive the system to be more metallic since the energy level of Pd $4d$ orbitals are higher than that of Ni $3d$ orbitals, however, it is not appropriated for the study. It is reported that 100 % palladium substituted compound, Ta_2PdS_5 , crystallizes in a different crystal structure (see Fig. 2-2). In Ta_2PdS_5 , the tantalum atoms are trigonal prismatic coordinated while Pd has square planer coordination, respectively.

Instead, it is discovered that Ta_2PdS_5 undergoes a superconducting transition at around $T_c \sim 6$ K and shows large upper critical field even beyond Pauli limit. The physical properties of Ta_2PdS_5 will also be discussed in chapter 6 [33,46].



(C)

	Ni	Pd
S	Ta ₂ NiS ₅	Ta ₂ PdS ₅
Se	Ta ₂ NiSe ₅	-

semiconductor
 semi-metal

Figure 2-2: (A) The crystal structure of Ta₂NiSe₅ and (B) Ta₂PdS₅. When the Ni site is 100 % substituted by Pd atoms, the system hold different crystal structure and shows semi-metallic behavior which is summarized in (C).

Chapter 3 Experimental

3. 1 Sample preparation and characterization of Ta_2NiCh_5 (Ch = sulfur, selenium and tellurium)

Single crystals of Ta_2NiCh_5 (Ch = sulfur, selenium and tellurium) are grown by using chemical vapor transport method as mentioned by F. J. DiSalvo et al [42]. Elemental powders of tantalum, nickel and chalcogens (sulfur, selenium and tellurium) were mixed with a stoichiometric ratio and sealed into an evacuated quartz tube ($\sim 10^{-3}$ Pa) with small amount of iodine as transport agent. The mixture was sintered under a temperature gradient of 950/850 °C as shown in Fig. 3-1 (A). After sintering for 1 week, needle-like single crystals were grown at the cold end of the tubes (see Fig. 3-1 (B)). The needle-like crystals are stable in air. The obtained crystals were characterized by X-ray diffraction (XRD) at room temperature using Cu- $K\alpha$ radiation (Rigaku RINT Ultima III). The sulfur content of $Ta_2Ni(Se_{1-x}S_x)_5$ crystals were measured by using SEM/EDX (Keyence).

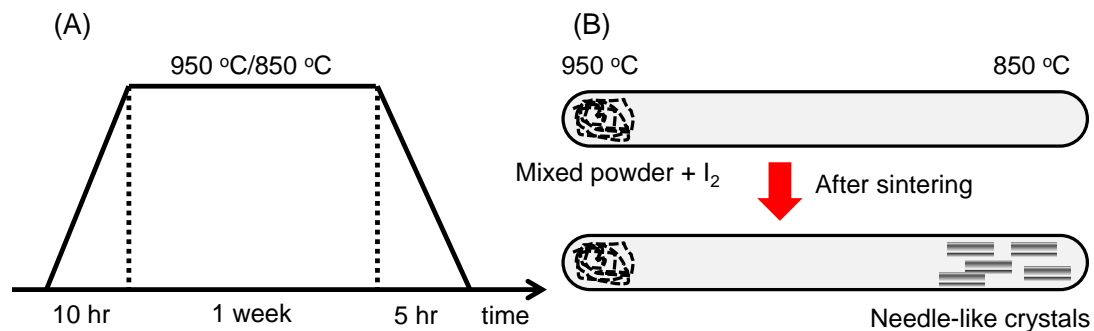


Figure 3-1: (A) Schematic picture of synthesis condition of Ta_2NiSe_5 . (B) The elemental powder of tantalum, nickel and selenium are mixed and sealed into evacuated quartz tube. After sintering for 1 week, needle-like silver crystals were grown at the cold end of the tube.

Fig. 3-2 (A) and (C) show the experimental XRD data of sulfur and tellurium substituted Ta_2NiSe_5 . The peaks of $(0\ b\ 0)$ ($b = 2, 4, 6, 8$ and 10) are found to be emphasized, implying that the crystals are highly oriented along the b -direction. By using the obtained peaks, lattice constant of sulfur and tellurium substituted Ta_2NiSe_5 were calculated which is summarized in Fig. 3-2 (B) and (D). It is discovered that lattice constant of $Ta_2Ni(Se_{1-x}S_x)_5$ shrinks as sulfur content increases while tellurium

substitution enlarges lattice constant. It is concluded that chemical substituted Ta_2NiSe_5 were successfully synthesized since the change of lattice constant follow Vegard's rule.

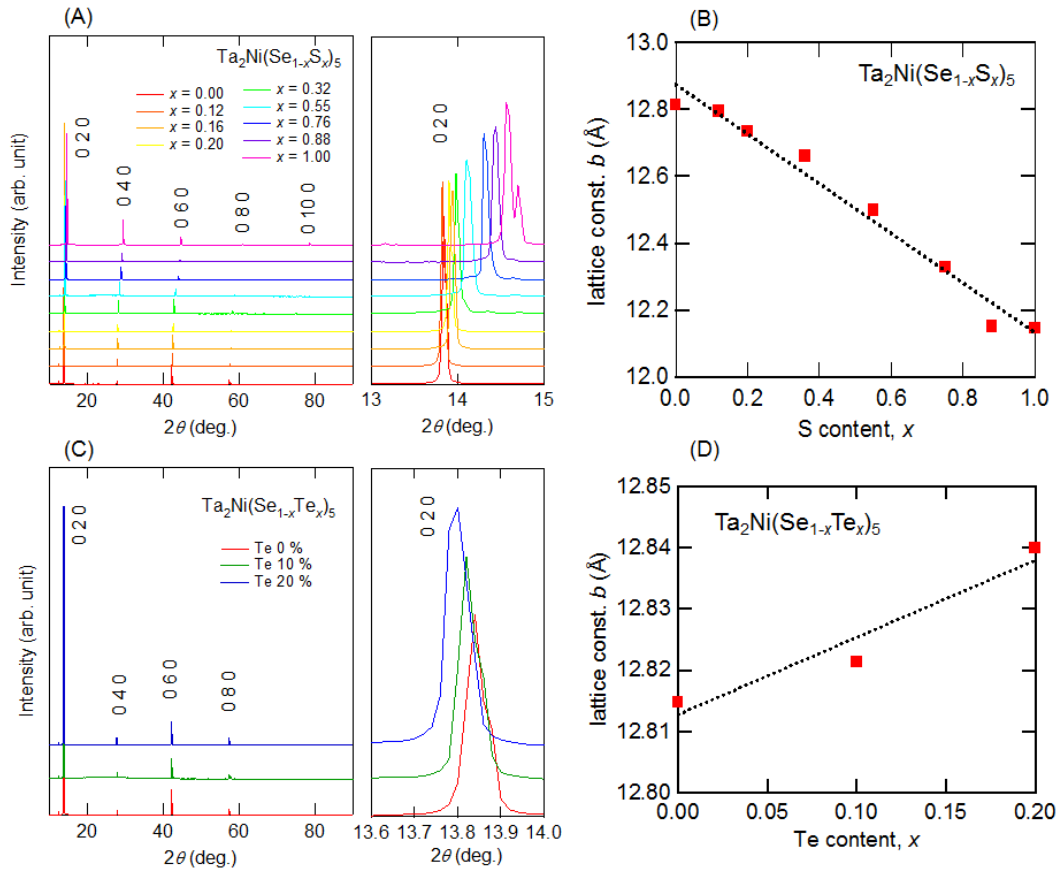


Figure 3-2: (A) X-Ray diffraction pattern of sulfur substituted Ta_2NiSe_5 taken at room temperature. The $0b0$ peaks are significantly emphasized and each peak is found to shift systematically towards higher 2θ angle. (B) Calculated lattice parameter b as a function of sulfur content, x , and can well be described by Vegard's law.

3. 2 Sample preparation and characterization of $\text{Ta}_2\text{Pd}_x\text{S}_5$

The polycrystalline samples of $\text{Ta}_2\text{Pd}_x\text{S}_5$ used in the study were synthesized by a conventional solid state reaction as reported by P. J. Squattritto et al [46]. Elemental powders of tantalum, palladium and sulfur were mixed and pelletized with a starting composition of $2 : x_{nom} : 5$. Here x_{nom} denotes nominal palladium contents such as 1.10, 1.05 and 0.99. The 10 % excess palladium was needed for suppressing palladium deficiencies. The pellets were sealed into an Ar-filled quartz tube, and heated up to 400 °C. The tubes were subsequently slowly heated to 820 °C to avoid rapid

volatilization of sulfur and sintered for 30 hours. The obtained samples were black and stable in air.

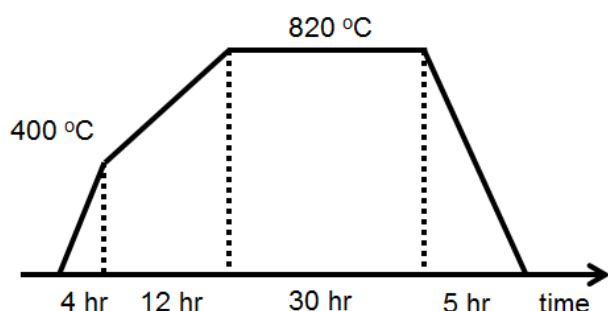


Figure 3-3: (A) Schematic picture of synthesis condition of Ta₂NiSe₅. The tubes were slowly heated up to 400 °C, and subsequently heated to 820 °C to avoid rapid volatilization of sulfur.

The obtained polycrystalline samples of Ta₂Pd_xS₅ were characterized by using powder X-ray diffraction with 2θ of 10 to 90 degrees. Fig. 3-4 shows the experimental data of Ta₂Pd_xS₅. The XRD pattern of the Ta₂Pd_xS₅ polycrystalline samples showed that the obtained powder was almost single phase with a small trace of TaS₂. The result of Rietveld refinement indicated the presence of palladium deficiency and the palladium content x were determined to be 0.97, 0.94 and 0.89, respectively. A systematic change of lattice constants as a function of x was observed, indicating that the amount of palladium deficiencies can be controlled.

3. 3 Transport, optical and thermodynamic properties

Electric resistivity and heat capacity measurement were measured by using PPMS (Quantum Design). High temperature electronic resistivity was measured by using handmade measurement devices. The pressure experiment is performed by Mr. H. Kono by using pressure cell (GPC-33, ElectroLab). The sample holder is composed by Teflon cell and Daphne oil is used as pressure transmission. Ta₂NiSe₅ single crystals are loaded into the sample cell with pure tin in order to monitor the magnitude of effective pressure. Optical conductivity is measured by Prof. Keimer's group (MPI, Germany) by using spectroscopic ellipsometry.

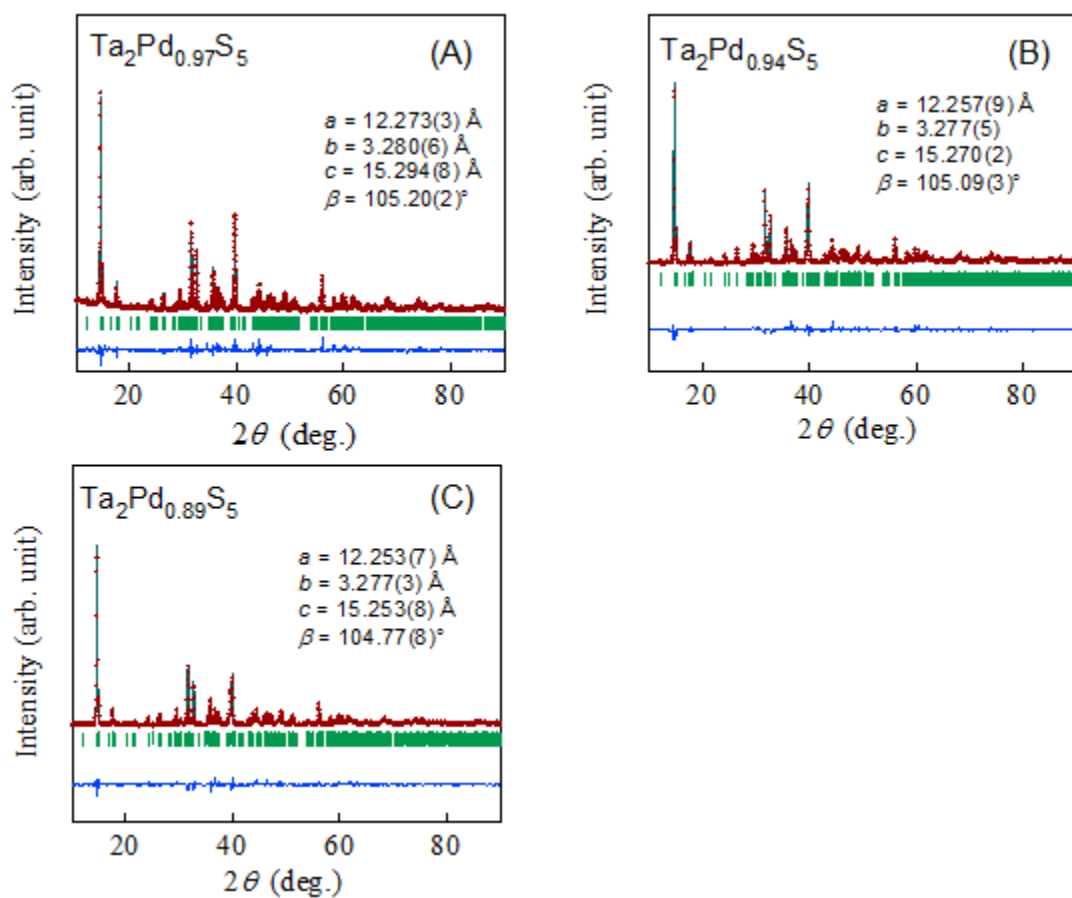


Figure 3-4: XRD pattern of the $\text{Ta}_2\text{Pd}_x\text{S}_5$ polycrystalline samples recorded by using $\text{Cu-K}\alpha$ radiation at room temperature. The red crosses, black solid line, lower green bars and blue solid line represent the experimental data, calculated pattern, expected peak positions and the difference between the experimental data and calculated pattern, respectively. The reliability factors of each analysis were obtained to be (A) $R_{\text{wp}} = 8.841\%$, $R_e = 4.225\%$, (B) $R_{\text{wp}} = 11.310\%$, $R_e = 7.450\%$, (C) $R_{\text{wp}} = 11.536\%$, $R_e = 7.657\%$, respectively.

Chapter 4 Basic physical properties of Ta₂NiSe₅

Excitonic insulator is an electronically driven phase originated from exciton condensation. It is discussed that exciton condensation can be described in analogy with BCS theory of superconductivity [10]. However, since exciton only has zero-charge, neither zero resistance nor Meissner effect is predicted in an excitonic insulator. This makes difficult to identify the presence of excitonic insulator state since the physical properties of excitonic insulator is similar to that of CDW state [8,9]. To this end, it is ineludible to identify the excitonic gap 2Δ and entropy change associated with the phase transition since both of them are the generic characters of an excitonic insulator. While TmSe_{0.45}Te_{0.55} and 1T-TiSe₂ have been studied as excitonic insulator candidates, neither of them has been identified due to the effect of a lattice distortion and a magnetic transition [27,37]. In order to avoid the difficulties, we focused on the recently discovered excitonic insulator candidate material Ta₂NiSe₅ which is reported to be a narrow gap semiconductor with direct gap system at Γ point ($\mathbf{q} = 0$) in the momentum space [42-44].

In this chapter, we report the transport, thermodynamic and optical properties of Ta₂NiSe₅. It is discovered that Ta₂NiSe₅ is a close-to-zero gap semiconductor in the high temperature phase and the system become a non-magnetic insulating state below T_c , evidenced by electronic resistivity and magnetic susceptibility anomalies. Interestingly, it is discovered that the in-plane resistivity of Ta₂NiSe₅ becomes more isotropic in the low temperature phase whereas band calculation predicts quasi-one dimensional characters of both conduction and valence bands. We argue that more isotropic in-plane electronic conductivity is realized by electron-hole hybridization between conduction and valence band which should result in additional gap formation in the Fermi level. The magnitude of the gap 2Δ in the low temperature phase is directly measured by using optical conductivity, giving $2\Delta = 0.3 - 0.4$ eV. The phase transition of Ta₂NiSe₅ was furthermore confirmed by thermodynamic properties. A clear anomaly can be identified at T_c in our heat capacity measurement. The entropy change associated with the phase transition is calculated to be $\Delta S \sim 0.6$ J/(mol K). This corresponds to approximately 7 % of gas constant and strongly suggests that the phase transition is dominated by the electronic system. The discovery of clear gap formation and electronic heat capacity anomaly is the first example among the excitonic insulator candidate materials which is in good agreement with excitonic insulator transition.

4. 1 Anisotropic in-plane resistivity in Ta₂NiSe₅

Here we report the temperature dependence of in-plane electronic resistivity anisotropy, ρ_c/ρ_a . Fig. 4-1 (A) shows the electronic resistivity of Ta₂NiSe₅ single crystal in the temperature range from 350 K to 2 K. The electronic current is applied along the *a*-axis (parallel to the quasi-one dimensional chains, red) and *c*-axis (perpendicular to the quasi-one dimensional chains, blue), respectively. The in-plane resistivity is anisotropic and ρ_c/ρ_a is estimated to be approximately ~ 6 at 350 K, possibly reflecting quasi-one dimensional band structure (see Fig. 4-1 (B)). It is more conductive when the electronic current is applied along the *a*-axis, consistent with band calculation. Ta₂NiSe₅ shows semiconductor-like temperature dependence below 350 K and it undergoes a semiconductor-to-insulator transition at 326 K which is evidenced by electronic resistivity anomaly. We show the activation energy plot of Ta₂NiSe₅ in the inset of Fig. 4-1 (A) which is calculated by using following definition,

$$E_\rho = -T^2 \times \left(\frac{d \ln \rho}{dT} \right) (\text{K}) \quad (4-1)$$

Since the equation contains derivative term, the electronic resistivity anomaly is emphasized and clear peak appears at the point of T_c (see the inset of Fig. 4-1 (A)). In this thesis, we define T_c of the transition at middle point of the anomaly in the activation energy plot. Since the electronic resistivity of excitonic insulator state is described by the equation (1-1), the E_ρ versus T plot is considered to decay below T_c [13]. Interestingly, the resistivity anomaly is significant when the electronic current is applied along the *a*-axis while the electronic resistivity along the *c*-axis is less affected by the phase transition. Consequently, more isotropic in-plane resistivity is realized below the T_c (See Fig. 4-1 (B)). It might be originated from the electron-hole hybridization which will be discussed later (Chapter 7).

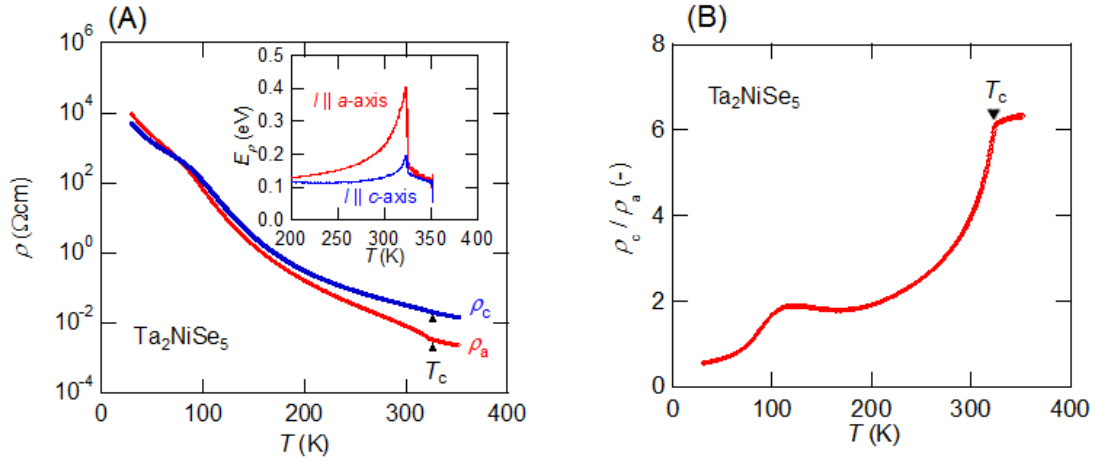


Figure 4-1: (A) In-plane electronic resistivity of Ta_2NiSe_5 as a function of temperature. The electronic current is applied along the quasi-one dimensional chains ($I \parallel a$ -axis) and perpendicular to the chains ($I \parallel c$ -axis) which are depicted as red and blue lines, respectively. (B) The magnitude of electronic resistivity anomaly ρ_c/ρ_a as a function of temperature. The magnitude of ρ_c/ρ_a is found to be significantly suppressed below T_c .

4. 2 Carrier density of Ta_2NiSe_5

The gap formation in Ta_2NiSe_5 below T_c also can be identified by Hall measurements. Fig. 4-2 shows the measured Hall resistivity $\Delta\rho_{xy}$ and estimated carrier density of Ta_2NiSe_5 as a function of temperature. At 350 K, the carrier density is calculated to be the order of $n \sim 8 \times 10^{20} \text{ cm}^{-3}$ which is close to some semi-metallic chalcogenides such as $1T\text{-TiSe}_2$ ($n \sim 3 \times 10^{20} \text{ cm}^{-3}$ at 300 K). The effective carrier density is found to be suppressed as temperature is lowered, which is estimated to be $n \sim 10^{16} \text{ cm}^{-3}$ at 100 K. Intriguingly, it is discovered that sign of Hall coefficient changes at approximately 150 K, indicating the co-existence of electron and hole. We argue that the sign change of Hall coefficient does not originate from any phase transitions. No heat capacity, magnetic susceptibility and electronic resistivity anomalies can be identified at corresponding temperature.

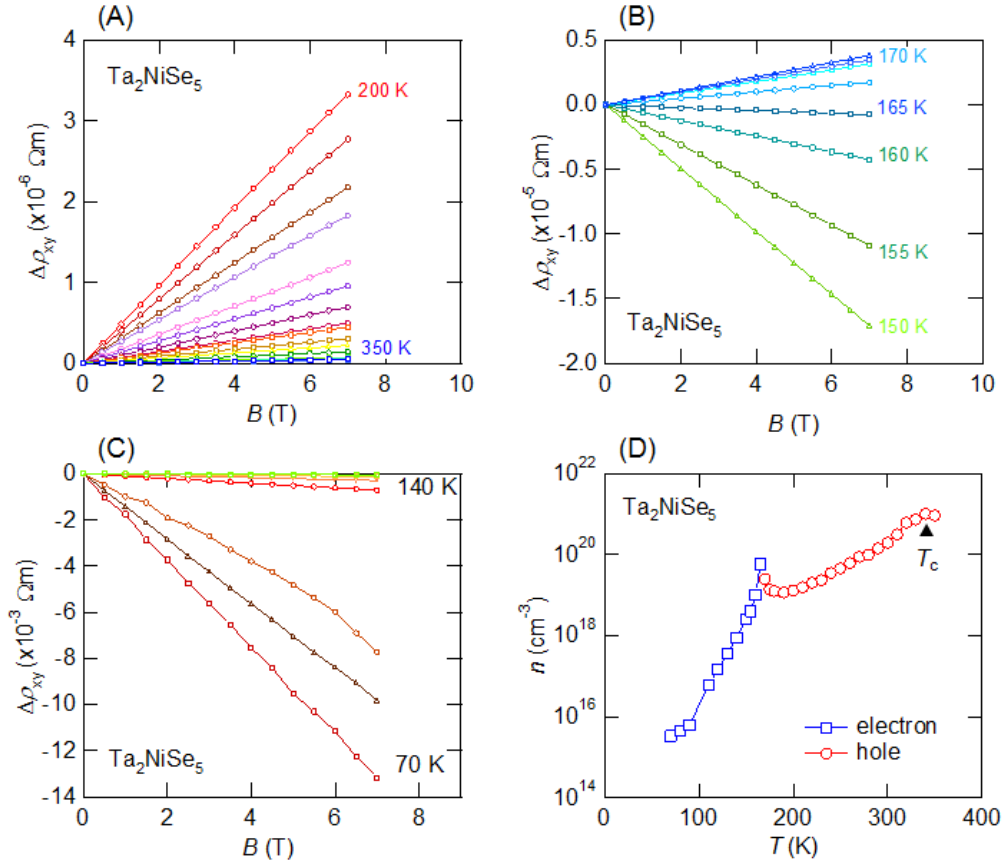


Figure 4-2: (A) The measured Hall resistivity $\Delta\rho_{xy}$ in the temperature range of 350 K to 200 K, (B) 170 K to 150 K and (C) 140 K to 70 K, respectively. (D) The calculated carrier density of pure Ta₂NiSe₅ as a function of temperature. The carrier density is found to decrease below T_c , indicating gap formation at Fermi level. The black triangle shows T_c .

4. 3 High temperature transport properties of Ta₂NiSe₅

The magnitude of activation energy in the high temperature phase of Ta₂NiSe₅ is one of the most important physical parameters for gap evaluation in the conduction and valence bands. K. Seki et al. reported band dispersion of the valence band along the X- Γ -X direction by using ARPES technique at 340 K [11]. Surprisingly, it is clearly seen that finite gap opens even above T_c of the phase transition, suggesting a pseudo-gap formation (see Fig. 1-14). The pseudo-gap formation in Ta₂NiSe₅ is furthermore suggested from magnetic susceptibility measurement. It is discovered by F. J. DiSalvo et al. that magnetic susceptibility starts decaying below 450 K which is approximately 120 K higher than T_c [42]. Therefore, in order to evaluate the magnitude

of activation energy of Ta_2NiSe_5 , it is demanded to measure high temperature transport properties. Here we show the electronic resistivity up to 550 K and its corresponding Arrhenius plot in Fig. 4-3. The high temperature resistivity measurements were performed by using four-probe method in the hand-made measurement system. The electronic current is applied along the a -axis. The electronic resistivity increases as temperature is lowered, consistent with the previous study [42]. Reflecting the pseudo-gap formation, Arrhenius plot is discovered to be temperature dependent as shown in Fig. 4-3 (B). We calculated its activation energy by using the points in the temperature ranges of 500 K to 550 K in order to avoid the effect of pseudo-gap formation. This gives activation energy of Ta_2NiSe_5 to be 0.01 eV (see the inset of Fig. 4-3 (A)). The co-existence of electron and hole, found in Hall measurement, is furthermore consistent with the close-to-zero gap picture. Ta_2NiSe_5 is therefore can be regarded as a zero gap semiconductor.

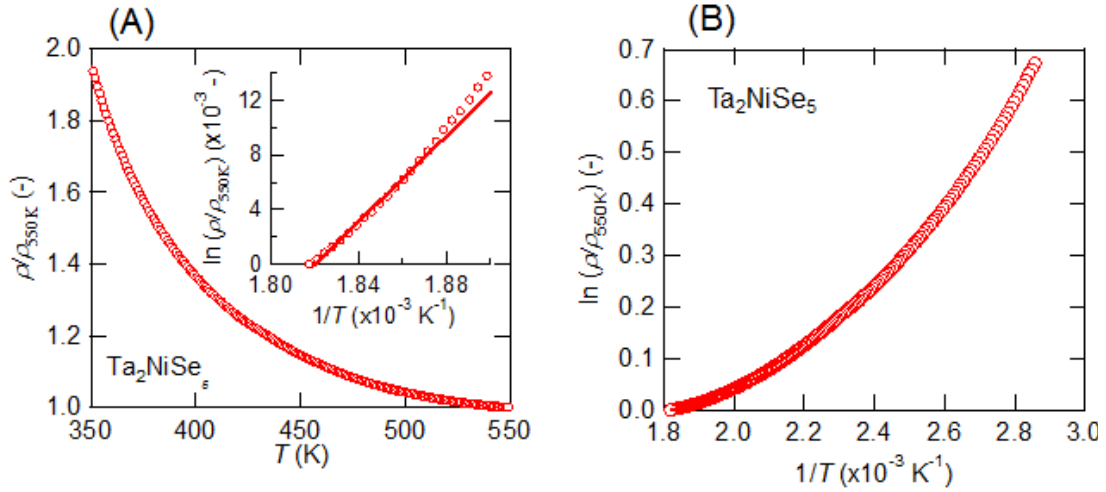


Figure 4-3: (A) High temperature electronic resistivity of Ta_2NiSe_5 . The electronic resistivity is renormalized at 550 K. The inset represents the Arrhenius plot in the temperature range of 500 to 550 K. (B) Corresponding Arrhenius plot of Ta_2NiSe_5 from 350 to 550 K. The activation energy is found to be temperature dependent even above T_c .

4. 4 Optical conductivity of Ta_2NiSe_5

The gap formation in Ta_2NiSe_5 is furthermore evidenced by optical conductivity shown in Fig. 4-4ⁱⁱⁱ. At 350 K, a small activation energy as large as ~ 0.1

ⁱⁱⁱ The optical conductivity is measured by Prof. Keimer's group (MPI, Stuttgart) by using spectroscopic ellipsometry method.

eV can be identified from transport experiments which may be associated with pseudo-gap feature, and therefore no Drude peak can be seen in the optical conductivity even above T_c . At 10 K, the gap becomes more significant from 0.3 eV point and show a maximum point at 0.4 eV (see Fig. 4-4). Since the activation energy of Ta_2NiSe_5 above T_c is much smaller than 0.3 - 0.4 eV, this should predominantly reflect the magnitude of 2Δ . Taking the value into account with observed T_c , the transition is in the strong coupling regime with $2\Delta/k_B T_c = 13 - 15$. According to the previous ARPES studies, it is discussed that the gap is as large as 0.17 eV in the valence band [11]. This implies that there should be at least 0.12 eV gap formation in the conduction band in order to explain the magnitude of 2Δ obtained from optical conductivity measurement. This is in strong contrast to the $1T\text{-TiSe}_2$ case which lowers the energy level of both conduction band and valence bands below T_c .

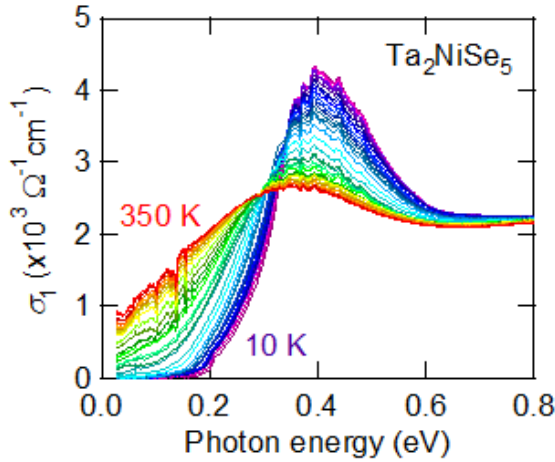


Figure 4-4: Optical conductivity of Ta_2NiSe_5 obtained by using spectroscopic ellipsometry method. Clear gap formation can be identified below T_c . The black triangle shows the point gap 2Δ , which is estimated to be 0.3 - 0.4 eV.

4.5 Specific heat anomaly at T_c

The excitonic gap formation should make a significant change in the thermodynamic properties. In order to estimate the entropy change associated with the phase transition, we carried out a heat capacity measurement as shown in Fig. 4-5. A pronounced anomaly is identified at T_c . We estimated the lattice contribution to heat capacity, C_{lattice} , by using the two Debye functions,

$$C_{\text{lattice}} = (8-a) \times 9R \left(\frac{T}{\theta_{D1}} \right)^3 \int_0^{\theta_{D1}/T} dx \frac{x^4 e^x}{(e^x - 1)^2} + a \times 9R \left(\frac{T}{\theta_{D2}} \right)^3 \int_0^{\theta_{D2}/T} dx \frac{x^4 e^x}{(e^x - 1)^2} \quad (4-2)$$

where R , θ_{D1} and θ_{D2} denote gas constant and Debye temperatures, respectively. Each of the parameters are obtained from the fitting of the experimental data below T_c which

gives $a = 1.571$, Debye temperature $\theta_{D1} = 354.0$ K and $\theta_{D2} = 130.4$ K, respectively. The several Debye temperatures in Ta_2NiSe_5 indicate the presence of anisotropic phonon spectrum. As shown in Fig. 1-9, Ta_2NiSe_5 is a layered material and each Ta_2NiSe_5 layer is composed of quasi-one dimensional chains of corner shared $NiSe_4$ tetrahedra and edge shared $TaSe_6$ octahedra. While more ionic bonding is expected between tantalum-selenium, nickel-selenium bonding should be more isovalent due to the difference of ionic tendency. The low dimensionality of the lattice and chemical bonding should give rise to the complex and anisotropic phonon spectrum and therefore several Debye temperatures are required to well explain the heat capacity contributed by lattice system, $C_{lattice}$.

Fig. 4-5 (B) shows the electronic heat capacity contribution C_{el}/T as a function of temperature. The electronic heat capacity C_{el} was calculated by subtracting $C_{lattice}$ from the obtained value. The result, plotted as C_{el}/T versus T , shows a clear jump at T_c and the C_{el} anomaly is reminiscent of a BCS-type superconducting transition, expected due to the formal analogy of the theories [10,11]. The entropy change associated with the transition is estimated to be $\Delta S \sim 0.6$ J/(mol K) by integrating C_{el}/T as a function of temperature up to T_c .

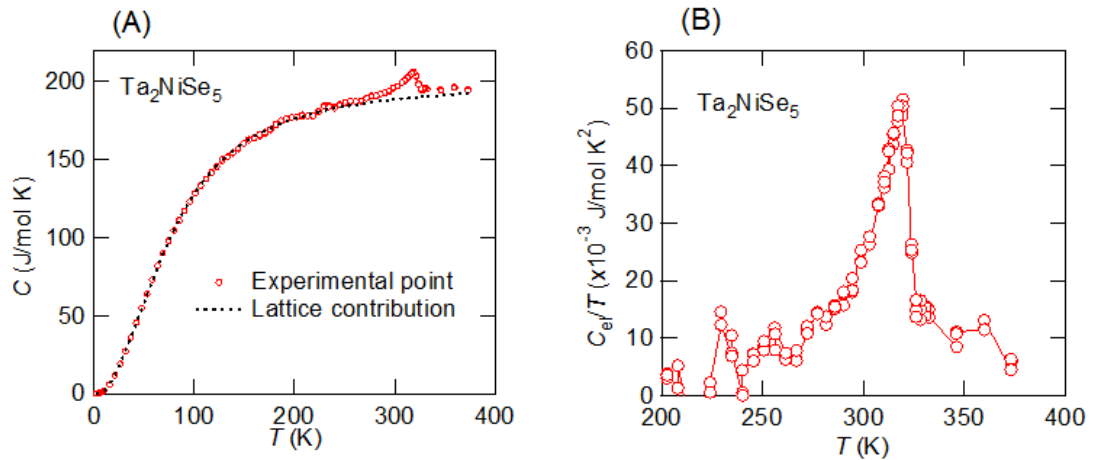


Figure 4-5: (A) Heat capacity of Ta_2NiSe_5 as a function of temperature. The red circle and black dashed line denote experimental points and calculated lattice contribution, respectively. (B) Electronic heat capacity C_{el} divided by temperature obtained by subtracting lattice contribution.

4. 6 Discussion of the chapter

The transport and optical conductivity measurements show that the high

temperature phase of Ta_2NiSe_5 is a close-to-zero gap system and electron-hole hybridization appears below T_c . Obtained heat capacity data also constitute thermodynamic evidence for the opening of a large gap in the electronic excitation spectrum. A pronounced anomaly can be identified in the electronic heat capacity at T_c and entropy change associated with the phase transition is estimated to be at least $\Delta S \sim 0.6 \text{ J}/(\text{mol K})$ by integration of the heat capacity anomaly. This magnitude corresponds to approximately 7 % of gas constant and it is clearly too large to be accounted for only as contribution from the lattice degree of freedom. We argue that such large entropy change is only possible by assuming exciton condensation which will be discussed in the chapter 7.

While such large entropy change should be a generic feature of an excitonic insulator transition, we are only aware of one further candidate material, $\text{Tm}(\text{Se}_{0.45}\text{Te}_{0.55})$, where changes of a similar order of magnitude have been reported [37]. In this case, however, it is discussed that changes in ΔS contain significant contributions from the lattice heat capacity and additional changes in the spin state of the Tm ion. Neither of these are relevant for Ta_2NiSe_5 , and thus the cleanest semiconductor-to-insulator transition is realized in the system which can be described by the excitonic insulator scenario.

4. 7 Summary of the chapter

In summary, we have measured transport, optical and thermodynamic properties of Ta_2NiSe_5 . Ta_2NiSe_5 is discovered to be a close-to-zero gap system and undergoes a phase transition with electron-hole hybridization. Below T_c , the magnitude of the gap was obtained to be $2\Delta = 0.3 - 0.4 \text{ eV}$ from our optical conductivity measurement, indicating that the phase transition is in strong coupling regime $2\Delta/k_B T_c = 13 - 15$. Crucially, we first observed the gap formation in the conduction band which cannot be accessed only by ARPES technique. The obtained heat capacity data also constitute thermodynamic evidence for the opening of a excitonic gap in the electronic excitation spectrum. The entropy change associated with the phase transition is estimated to be $\Delta S \sim 0.6 \text{ J}/(\text{mol K})$ from the heat capacity measurement. Since the clear gap formation and an anomaly in the electronic heat capacity are the characteristic feature of an excitonic insulator, the phase transition of Ta_2NiSe_5 is in good agreement with excitonic insulator scenario.

Since the activation energy in the high temperature semiconducting phase is

considerably smaller than that of 2Δ , Ta_2NiSe_5 should be located at optimal point of the phase diagram as presented in Fig. 1-4. The strong coupling feature with $2\Delta/k_B T_c = 13 - 15$ is furthermore consistent with that Ta_2NiSe_5 locates at the optimal point. This opens up an opportunity to investigate the overall electronic phase diagram by driving the system towards either more insulating or metallic behaviour through pressure and chemical doping.

Chapter 5 Electronic phase diagram of Ta₂NiSe₅

It is discussed that T_c of excitonic insulator is strongly dependent on the magnitude of band gap E_G [8,9,14]. While an excitonic insulator state is expected to be the most stabilized at semi-metal/semiconductor boundary, i.e. $E_G \sim 0$, increased and decreased band gap E_G suppress T_c . In a semi-metallic region ($E_G < 0$), increased carrier density screens the Coulomb interaction between electron and hole, and consequently T_c is suppressed. This is in strong contrast to a simple hybridization gap which is expected to persist for large band overlap and finite electron density at Fermi level. For the semiconducting region ($E_G > 0$), exciton formation and condensation become thermodynamically unstable against the semiconducting ground state, and T_c is suppressed very quickly. Electronic phase diagram is one of the most characteristic features in excitonic insulators and therefore it can be a key experimental evidence of the presence of excitonic insulator.

Here we report the electronic phase diagram of Ta₂NiSe₅. As discussed in the last chapter, the magnitude of activation energy in Ta₂NiSe₅ is found to be as large as 0.01 eV, which is much smaller than the magnitude of excitonic gap 2Δ below T_c , implying that Ta₂NiSe₅ locates at optimal point of the phase diagram. This opens additional possibilities to investigate the characteristic phase diagram by tuning the magnitude of band gap into both semiconductor and semi-metallic side. In this chapter, we first report the effect of chemical substitution for tuning the magnitude of band gap. The physical properties of Ta₂NiS₅ is discussed and we show that sulfur substitution is useful to drive the system to be more insulating, resulting in suppression of T_c . Pressure effect, on the other hands, is employed to drive the system to be more metallic since it is the simplest and cleanest method to increase band overlap, i.e. band width. Again, the T_c is found to be suppressed as a function of pressure. Overall the T_c of Ta₂NiSe₅ is found to be suppressed as activation energy is both enhanced and decreased. Since Ta₂NiSe₅ is considered to locate at optimal point of the phase diagram, the obtained data is consistent with theoretical predictions and therefore can be one of the key experimental evidences which establishes excitonic insulator phase in the system.

5. 1 Activation energy of sulfur substituted Ta₂NiSe₅

The crystal structure of Ta₂NiS₅ is illustrated in Fig. 5-1 (A). Ta₂NiS₅ is an isostructural compound to Ta₂NiSe₅ in the high temperature phase. Ta₂NiS₅ crystallizes in the orthorhombic structure and each Ta₂NiS₅ layer is composed of quasi-one dimensional chains of edge shared TaS₆ octahedra and corner shared NiS₄ tetrahedra [41,42]. Due to the smaller ionic radius of sulfur, the lattice constant of Ta₂NiS₅ is smaller than that of Ta₂NiSe₅, and therefore Ta₂NiS₅ is expected to be more metallic from the aspect of chemical pressure. However, the band calculation indicates that Ta₂NiS₅ is a semiconductor with a larger band gap. Fig. 5-1 (B) shows the calculated band structure of Ta₂NiS₅ [47]. It is reported that the system is a semiconductor with a direct gap band structure at Γ point ($q = 0$). The valence band is composed by Ni 3d orbitals with S 3p admixture while the conduction band are dominated by Ta 5d orbitals, giving the oxidation state to be Ta⁵⁺, Ni⁰⁺ and S²⁻, respectively. The larger band gap in Ta₂NiS₅ cannot be interpreted from the aspect of chemical pressure effect. It is considered that the lower energy level of sulfur 3p orbitals play important role to enhance the band gap in this system. With increasing sulfur doping, the hybridization of valence band, between Ni 3d and Se 4p (S 3p) orbitals, is weakened. This lowers the energy level of the valence band while the conduction band is less affected, resulting in an overall enhancement of the energy gap compared to Ta₂NiSe₅. We note that more insulating character in sulfides than selenides and tellurides are widely seen in chalcogenide materials as represented in transition metal dichalcogenides, ZrCh₂ (Ch = sulfur, selenium and tellurium) [45].

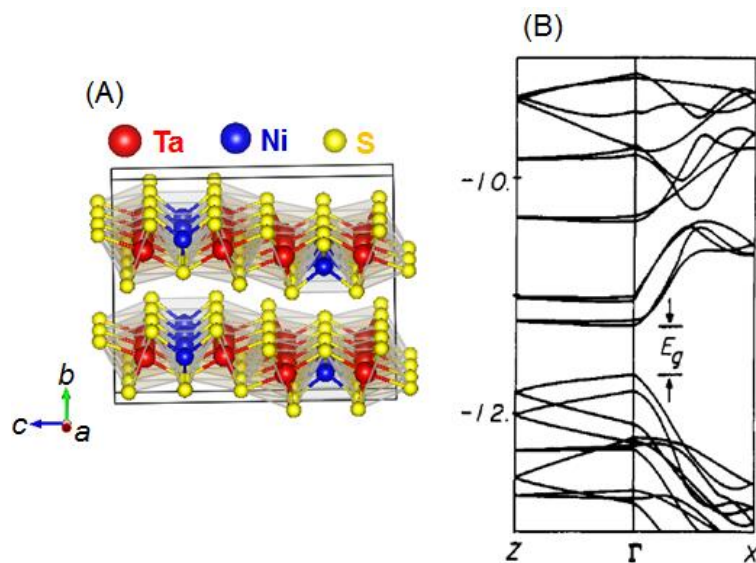


Figure 5-1: (A) The crystal and [41,42] (B) the band structure of Ta₂NiS₅ [47]. Ta₂NiS₅ is isostructural to Ta₂NiSe₅ and expected to be a direct gap semiconductor with a larger band gap E_G than that of Ta₂NiSe₅.

The more insulating behavior is experimentally confirmed by our high temperature electronic resistivity. Fig. 5-2 (A) shows the electronic resistivity of sulfur substituted Ta_2NiSe_5 renormalized at 550 K. The electronic current is applied along the a -axis (parallel to the quasi-one dimensional chains). While Ta_2NiSe_5 is a close-to-zero gap system, Ta_2NiS_5 is found to show a clear band gap as larger as $E_g \sim 0.17$ eV according to the corresponding Arrhenius plot (see Fig. 5-2 (B)). While Ta_2NiSe_5 undergoes a semiconductor-to-insulator transition at 326 K, no phase transitions can be identified down to 2 K in Ta_2NiS_5 . This implies that Ta_2NiS_5 is located outside of the semiconducting end of the proposed electronic phase diagram of excitonic insulator. Therefore, sulfur substitution into Ta_2NiSe_5 is expected to drive the system to be more insulating and gives the phase diagram of semiconductor side. We synthesized $\text{Ta}_2\text{Ni}(\text{Se}_{1-x}\text{S}_x)_5$ and estimated their activation energy by using high temperature electronic resistivity measurements. It is clearly seen that activation energy is systematically enhanced with increased sulfur content, x , which are summarized in the inset of Fig. 5-2 (B).

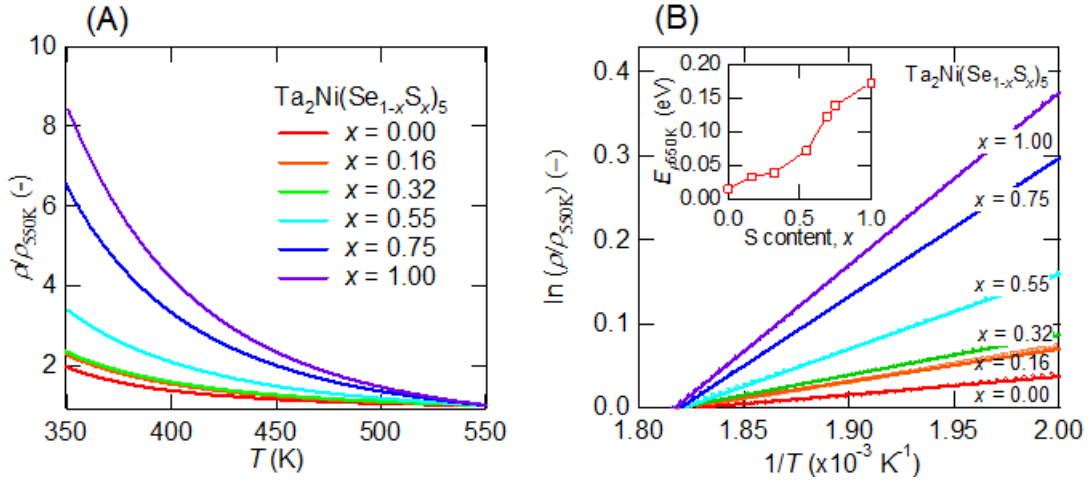


Figure 5-2: (A) High temperature electronic resistivity and (B) its corresponding Arrhenius plot of sulfur substituted Ta_2NiSe_5 . The activation energy is found to be enhanced systematically with increased sulfur content, x , which is summarized in the inset.

5. 2 T_c of chemical substituted Ta_2NiSe_5

Electronic resistivity below 350 K of sulfur doped Ta_2NiSe_5 were measured by using PPMS (Quantum Design). We show resistivity curves ($I \parallel a$ -axis) and the corresponding activation energy plots of $Ta_2Ni(Se_{1-x}S_x)_5$ in Fig. 5-3 (A) and (B). T_c of Ta_2NiSe_5 is discovered to be suppressed as sulfur content increases, i.e. activation energy enhances. Here it is apparent that not only is T_c suppressed but that furthermore the precursor upturn systematically diminishes gradually with increased sulfur doping. This might be related to a suppression of fluctuations in the high temperature phase predicted theoretically [11].

In order to tune the band structure towards the metallic end of the phase diagram (Fig. 1-4), we carried out an isovalent tellurium doping study. We synthesized single crystals of $Ta_2Ni(Se_{1-x}Te_x)_5$ for the range of $0 < x < 0.2$. Possibly due to the solubility limit associated with the different ionic radius between selenium and tellurium, larger tellurium substitution is not chemically stable. We confirmed the increase of metallicity as a function of tellurium doping by electric resistivity^{iv}. In Fig. 5-3 (C) and (D), we show the resistivity traces for selected samples (traces offset for clarity). Again a suppression of T_c is observed with increasing tellurium content. Overall these chemical doping experiments indicate that both an increase and decrease in E_G suppress T_c of the phase transitions, consistent with theoretical expectations [9].

^{iv} The electronic resistivity of $Ta_2Ni(Se_{0.8}Te_{0.2})_5$ at 350 K is approximately 20 % lower than that of pure Ta_2NiSe_5 .

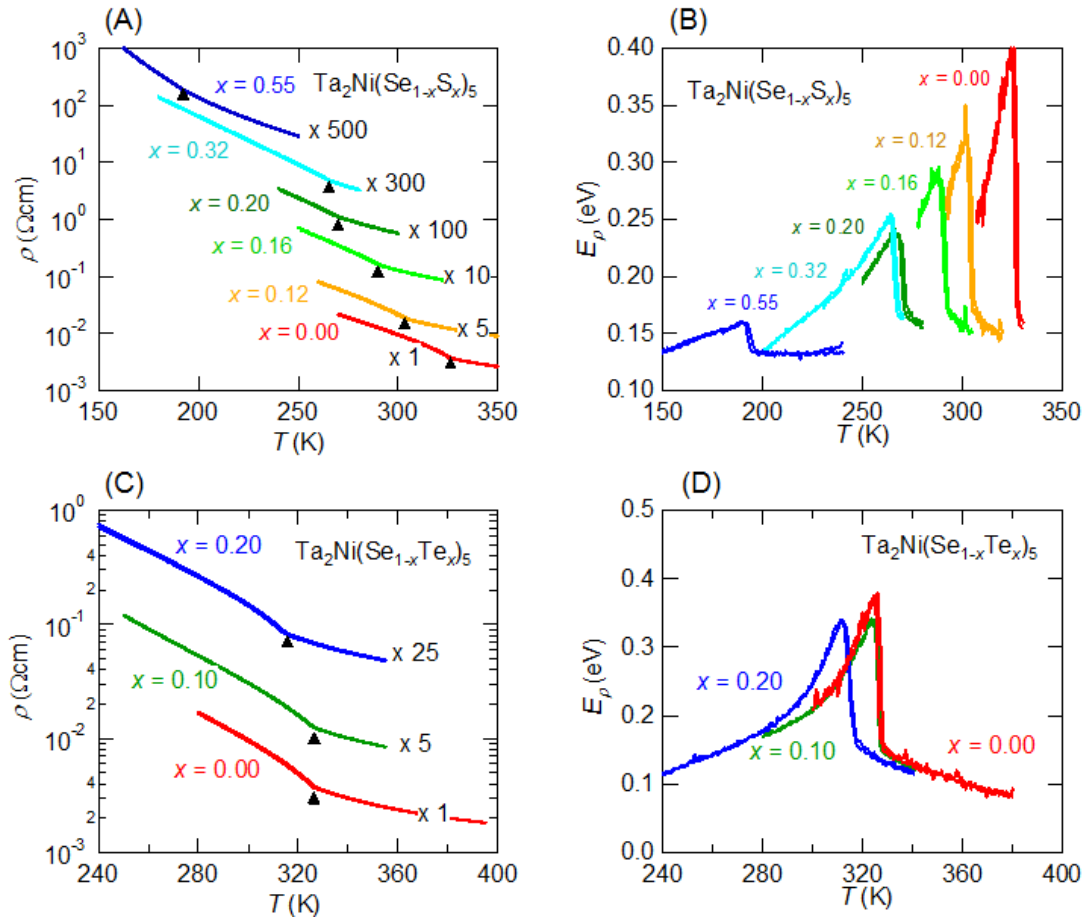


Figure 5-3: (A) Electronic resistivity ($I \parallel a$ -axis) as a function of temperature for single crystal Ta₂Ni(Se_{1-x}S_x)₅ in the selected temperature range. The curves are offset for clarity of presentation (corresponding tin a log plot to multiplication by 1, 5, 10, 100, 300 and 500 respectively). The black triangle marks indicate the point of T_c . (B) The corresponding E_g data of Ta₂Ni(Se_{1-x}S_x)₅, in which the transition shows up clearly. (C) In-plane resistivity as a function of temperature for single crystal Ta₂Ni(Se_{1-x}Te_x)₅. The curves are offset for clarity of presentation (corresponding tin a log plot to multiplication by 1, 5 and 25 respectively). Black triangles indicate T_c . (D) The corresponding E_g data of Ta₂Ni(Se_{1-x}Te_x)₅.

5. 3 Pressure effect of pure, sulfur and tellurium substituted

Ta_2NiSe_5

In order to further test this hypothesis, we carried out a range of hydrostatic pressure experiments. Since Ta_2NiSe_5 is a close-to-zero gap semiconductor, pressure effect is expected to drive the system into semi-metallic state. Fig. 5-4 (A) shows the electronic resistivity of pure Ta_2NiSe_5 as a function of temperature under pressure. With increased pressure, we indeed observe the systems to be more conductive. Above a pressure of 1.8 GPa, we observe the semiconductor-to-insulator transition at 293 K, corresponding to a T_c suppression rate of ~ 20 K/GPa^v. We note that the precursor upturn is quickly suppressed in the semi-metallic region. Even the T_c of pure Ta_2NiSe_5 at $P \sim 3$ GPa is same as sulfur 16 % doped Ta_2NiSe_5 , no precursor upturn can be seen under pressure while a clear pseudo-gap can be identified in $\text{Ta}_2\text{Ni}(\text{Se}_{0.84}\text{S}_{0.16})_5$. Increased pressure further lowers T_c until at ~ 3 GPa. At this pressure an additional phase transition into a semi-metallic phase is observed. It is noteworthy that all our pure, sulfur and tellurium doped Ta_2NiSe_5 samples show this pressure induced phase transition at approximately the same pressure $P \sim 3$ GPa. We therefore argue that it represents a separate instability of the lattice structure, which is independent of the excitonic insulator physics discussed here.

In Fig. 5-4 (C), we present the data of pressurising $\text{Ta}_2\text{Ni}(\text{Se}_{0.8}\text{Te}_{0.2})_5$. At this doping level, T_c at ambient conditions (red curve) is 317 K. Increased pressure both systematically reduces the resistivity (i.e. drives the sample more metallic) and lowers T_c consistent with our other experiments. Surprisingly, the pressure effect is found to be more complicated in sulfur doped systems. In Fig. 5-4 (E) and (F), we show the pressure dependence of resistivity in $\text{Ta}_2\text{Ni}(\text{Se}_{0.84}\text{S}_{0.16})_5$. Our initial expectation was that pressure would reverse the effect of sulfur doping and increase T_c . Contrary to this we observe that T_c is first suppressed by applying pressure and then enhanced at around $P \sim 1.2$ GPa. This implies that sulfur doping does not simply enhance the single particle gap E_G .

^v Electronic resistivity measurement under pressure is only available below 300 K since the sample holder of the pressure cell is made of Teflon. As temperature become higher, Teflon is softened and system cannot maintain pressure.

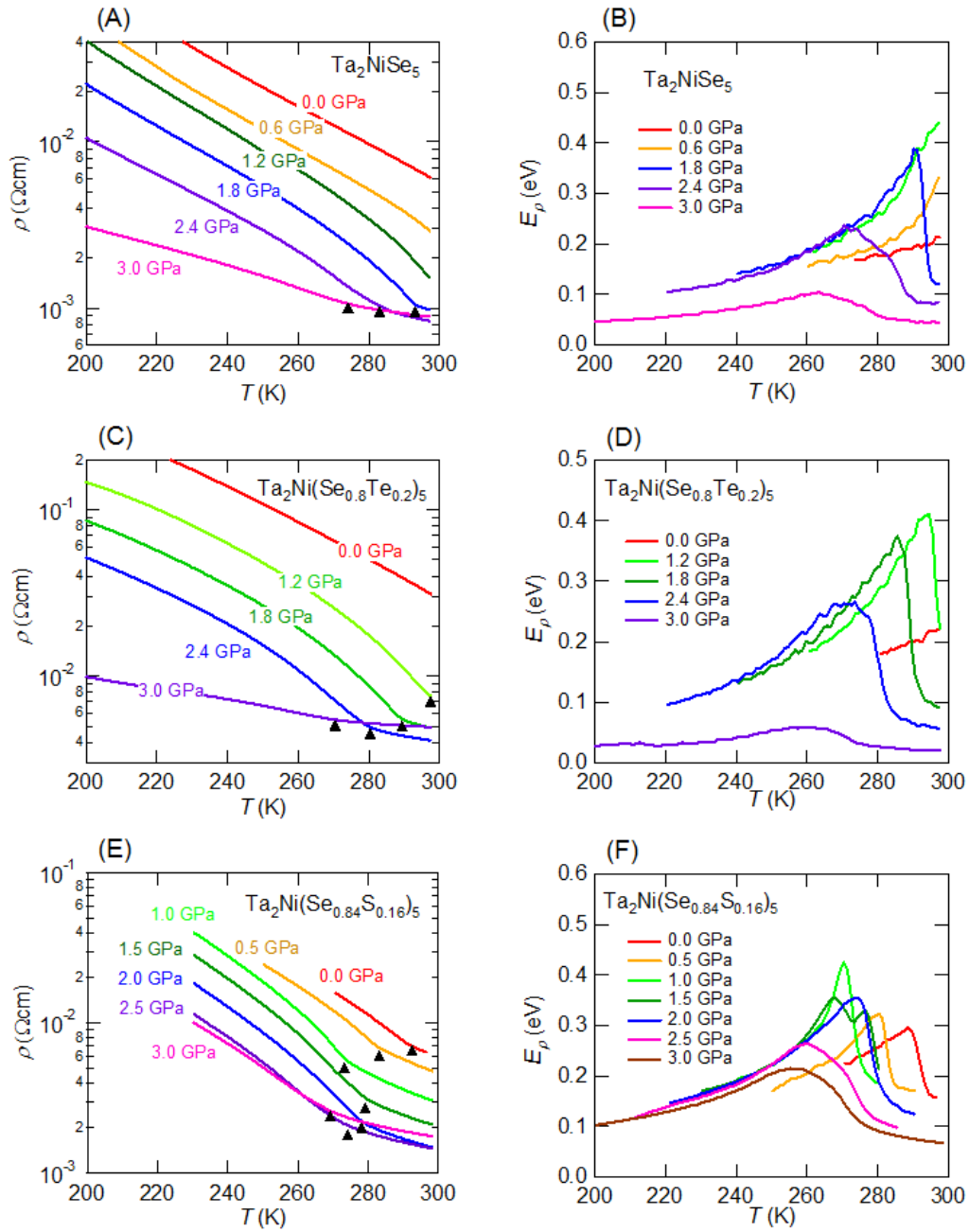


Figure 5-4: (A, C and E) Electronic resistivity ($I \parallel a$ -axis) as a function of temperature of single crystal Ta_2NiSe_5 , $\text{Ta}_2\text{Ni}(\text{Se}_{0.8}\text{Te}_{0.2})_5$ and $\text{Ta}_2\text{Ni}(\text{Se}_{0.84}\text{S}_{0.16})_5$ for a select range of pressures. Black triangles indicate T_c . (B, D and F) The corresponding E_g as a function of temperature of pure Ta_2NiSe_5 , $\text{Ta}_2\text{Ni}(\text{Se}_{0.8}\text{Te}_{0.2})_5$ and $\text{Ta}_2\text{Ni}(\text{Se}_{0.84}\text{S}_{0.16})_5$, respectively. In some cases a doubling of the transition can be observed which we attribute to pressure inhomogeneity. This however does not invalidate our general conclusions.

5. 4 Discussion of the chapter

Direct and close-to-zero gap band structure put Ta_2NiSe_5 very close to optimal conditions within the excitonic insulator scenario which motivates our explorations of the electronic phase diagram via chemical doping and pressure effects. Hydrostatic pressure only changes the magnitude of overlap between conduction and valence bands which tunes band gap directly without introducing any crystal imperfections. We observed that Ta_2NiSe_5 become more conductive as pressure increases with suppression of T_c . The primary aim of the complementary tellurium and sulfur doping studies was to extend the range of E_G . While tellurium substitution drives the system to be more metallic, activation energy is enhanced by sulfur substitution. It is discovered that both increased and decreased band gap E_G suppresses T_c of the phase transition, consistent with theoretical predictions of excitonic insulator [14].

The phase diagram of semi-metallic side is furthermore confirmed by applying pressure to tellurium doped Ta_2NiSe_5 . We observe an increase in electronic conductivity in combination with a decrease of T_c , placing these samples clearly on the semi-metallic side of the phase diagram. Sulfur doping is discovered to enhance the band gap in the high temperature phase as confirmed by our high temperature transport experiments. Hydrostatic pressure in principle should reverse the effect of sulfur doping and enhances T_c if band gap tuning was the primary effect of sulfur doping. Intriguingly, T_c is first suppressed and then enhanced by applying pressure in $\text{Ta}_2\text{Ni}(\text{Se}_{1-x}\text{S}_x)_5$ which is summarized in Fig. 5-5. We argue that these complicated pressure dependence originate from non-trivial effect of sulfur substitution. Since chemical substitution modified not only the band but also band character in the valence band which may reduce the electron-hole interaction which will be discussed later (chapter 7).

5. 5 Summary of the chapter

In summary, we have investigated and demonstrated the electronic phase diagram of Ta_2NiSe_5 by employing chemical substitution and pressure effects which is summarized in Fig. 5-5. While pressure and tellurium substitution drive the system to be more metallic, sulfur substitution is found to enhance magnitude of the band gap E_G , allowing us to access to the electronic phase diagram in the semiconducting side. T_c of Ta_2NiSe_5 was found to be suppressed by pressure, tellurium and sulfur doping effects. Since Ta_2NiSe_5 is considered to locate at optimal point of the phase diagram, the

obtained data is in good agreement with theoretical predictions. Pressure effect of tellurium and sulfur doped Ta_2NiSe_5 were also investigated. T_c of tellurium substituted Ta_2NiSe_5 is furthermore suppressed by applying pressure, consistent with theoretical predictions. Surprisingly, T_c of sulfur doped Ta_2NiSe_5 was found to be more complicated under pressure. While sulfur doping enhances magnitude of the band gap E_G , pressure effect is expected to reverse the effect and therefore enhance T_c in principle. Our experimental data shows that T_c of sulfur doped Ta_2NiSe_5 is first suppressed and then enhanced by applying pressure. This unexpected behavior can be attributed to non-trivial effects such as band (orbital) modification and impurity effects.

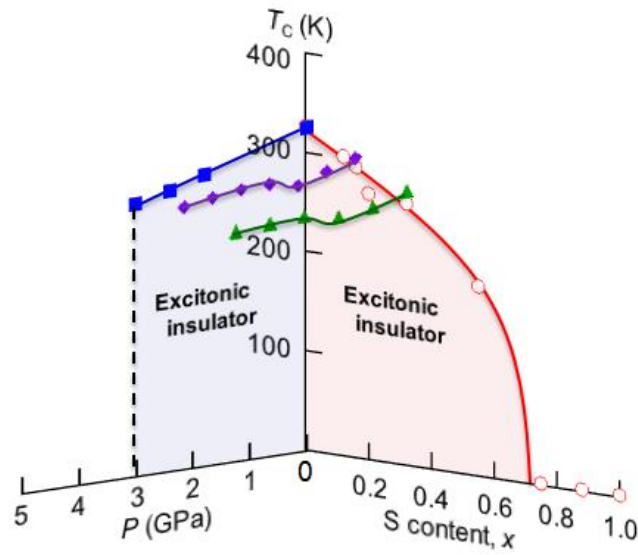


Figure 5-5: The phase diagram of the excitonic insulator phase in Ta_2NiSe_5 as functions of sulfur content (red) and pressure (blue), representing the semiconducting and semi-metallic region, respectively. The pressure effects on the $\text{Ta}_2\text{Ni}(\text{Se}_{1-x}\text{S}_x)_5$ (purple and green) are also shown. The dotted line indicates the 1st order phase transition at $P \sim 3$ GPa which we observed for all samples and therefore is a lattice instability unrelated to the excitonic insulator physics discussed in the study.

Chapter 6 Superconductivity in $\text{Ta}_2\text{Pd}_x\text{S}_5$

A superconducting phase proximity to an excitonic insulator has been theoretically discussed to be a prospective playground for exploring new high- T_c superconductors [18]. Since the energy scale of electron-hole interaction is much larger than that of phonon frequencies, P. Bhattacharyya et al. expected that a new high- T_c superconducting phase can manifest itself at the semi-metallic end of the phase diagram (see Fig. 6-1) [18]. In Ta_2NiSe_5 , however, system undergoes a pressure induced phase transition at approximately $P \sim 3$ GPa and therefore semi-metallic end of the phase diagram has not been achieved, yet.

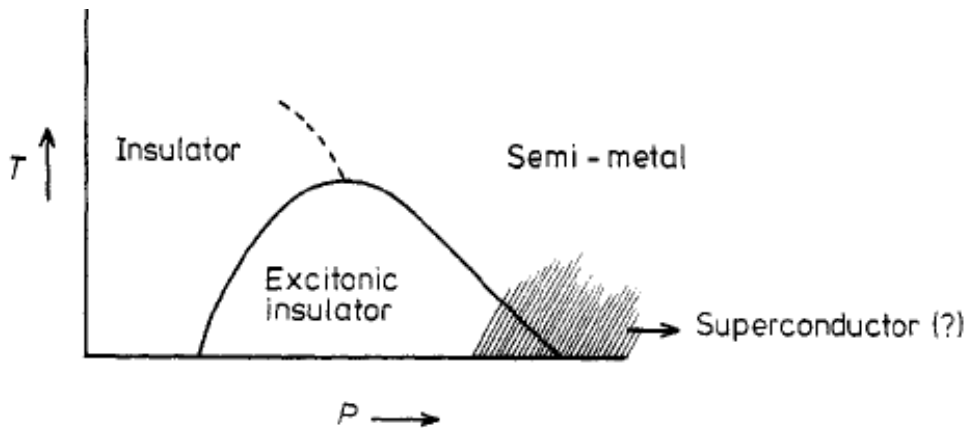


Figure 6-1: The theoretically predicted phase diagram of excitonic insulator. A new high- T_c superconducting phase is expected to manifest itself at the semi-metallic end of the phase diagram [18].

In this chapter, we report the transport, magnetic susceptibility and thermodynamic properties of $\text{Ta}_2\text{Pd}_x\text{S}_5$. The crystal structure of $\text{Ta}_2\text{Pd}_x\text{S}_5$ is different from that of Ta_2NiSe_5 , however, the electronic structure is found to be analogous. While Ta_2NiSe_5 is a close-to-zero gap system, $\text{Ta}_2\text{Pd}_x\text{S}_5$ is found to be a compensated metal. We discovered that $\text{Ta}_2\text{Pd}_x\text{S}_5$ undergoes a superconducting transition below $T_c \sim 6$ K, evidenced by zero resistance, Meissner effect and electronic heat capacity anomalies. The upper critical field of superconductivity (H_{c2}) in $\text{Ta}_2\text{Pd}_x\text{S}_5$ is found to be as large as 31 T at 0 K, exceeding the Pauli paramagnetic limit $\mu_0 H_P = 10.2$ T by a factor of 3. Since $\text{Ta}_2\text{Pd}_x\text{S}_5$ is considered to be a dirty-limit s -wave superconductor, we will discuss that the effect of spin-orbit scattering plays a significant role for suppressing paramagnetic pair breaking effect.

6. 1 The crystal and the electronic structure of $\text{Ta}_2\text{Pd}_x\text{S}_5$

The crystal and the electronic structure of $\text{Ta}_2\text{Pd}_x\text{S}_5$ are illustrated in Fig 6-2. $\text{Ta}_2\text{Pd}_x\text{S}_5$ was first synthesized by P. J. Squattorito et al. which were reported to be $\text{Ta}_2\text{Pd}_{0.89}\text{S}_5$ with palladium deficiencies [46]. Tantalum atoms are prismatically coordinated by six sulfur atoms, and the TaS_6 trigonal prism form quasi-one dimensional chains along the b -axis by sharing faces and edges while palladium atoms bridge the TaS_6 chains by forming PdS_4 square planer in between. There are two palladium sites, and one of them is not fully occupied. It is indicated by the published band calculation that the valence bands are composed of Pd $4d$ orbitals with S $3p$ admixture while Ta $5d$ orbitals dominate the conduction band [48]. It is pointed out that the system is a compensated metal since the calculation expects finite overlap between conduction and valence band (see Fig. 6-2 (B)) [48].

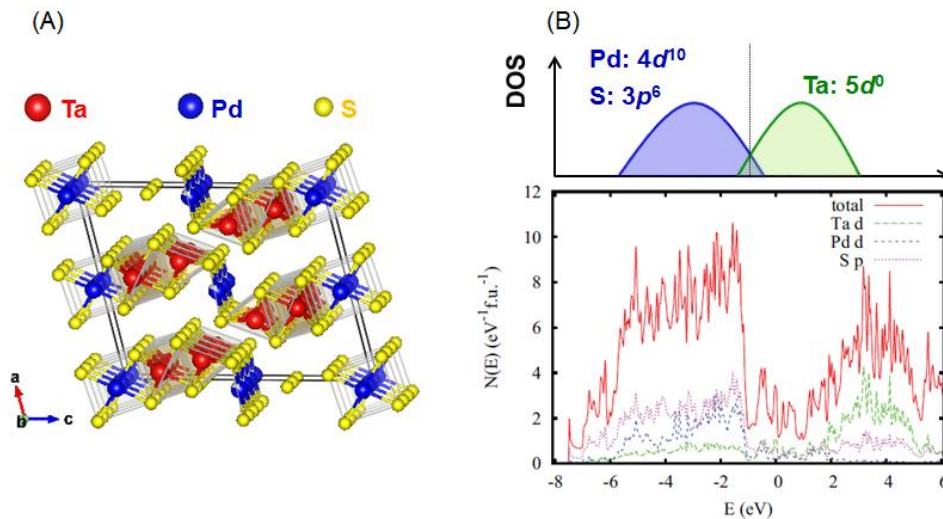


Figure 6-2: (A) Crystal structure of $\text{Ta}_2\text{Pd}_{0.89}\text{S}_5$ [46]. The tantalum atoms are prismatically coordinated by sulfur atoms and form quasi-one dimensional chains along the b -axis while palladium atoms are placed between the chains. (B) Calculated electronic density of state. It is discussed that $\text{Ta}_2\text{Pd}_x\text{S}_5$ is a semi-metal [48]. The conduction band is composed by Ta $5d$ orbitals while Pd $4d$ and S $3p$ orbitals dominate valence bands, respectively.

6. 2 Superconducting transition of $\text{Ta}_2\text{Pd}_x\text{S}_5$

Fig. 6-3 (A) and (B) show the electronic resistivity and magnetic susceptibility of $\text{Ta}_2\text{Pd}_x\text{S}_5$ as a function of temperature with different palladium content, x [49]. $\text{Ta}_2\text{Pd}_x\text{S}_5$ shows metallic conductivity and the carrier density is estimated to be $\sim 1 \times 10^{22}$

cm⁻³ from a Hall measurement. The obtained Hall coefficient is found to be temperature dependent, consistent with semi-metallic picture. Ta₂Pd_xS₅ undergoes a superconducting transition at $T_c \sim 6$ K as evidenced by zero resistance and Meissner effects. It is discovered that T_c depends on the palladium content, possibly due to chemical doping effect. Fig. 6-3 (C) shows the electronic heat capacity of Ta₂Pd_{0.97}S₅ as a function of temperature. The electronic and lattice contribution in the heat capacity was estimated by using the standard Debye model, $C(T) = \gamma T + \beta T^3$, by fitting $C(T)$ under magnetic field 12 T as shown in the inset of Fig. 6-3 (C). This yielded the electronic heat capacity coefficient and lattice contribution to be $\gamma = 27.6$ mJ/(mol K²) and $\beta = 1.25$ mJ/(mol K⁴), respectively. This gives Debye temperature θ_D of Ta₂Pd_{0.97}S₅ to be 231 K. The electronic heat capacity C_{el} is obtained by subtracting the calculated lattice contribution. A clear anomaly can be identified at around $T_c \sim 5.8$ K, hallmarking bulk superconductivity in Ta₂Pd_xS₅. The C_{el} anomaly is broadened possibly due to chemical inhomogeneity and it hinders our ability to reasonably fit the temperature dependence of C_{el} by using BCS theory. However, the rapidly diminishing $C_{el}(T)$ below T_c strongly suggests gap-full superconductivity. Combining this with the presence of strongly disordered lattice which suppresses sign-changing order parameter, it is concluded that Ta₂Pd_xS₅ hosts *s*-wave superconductivity.

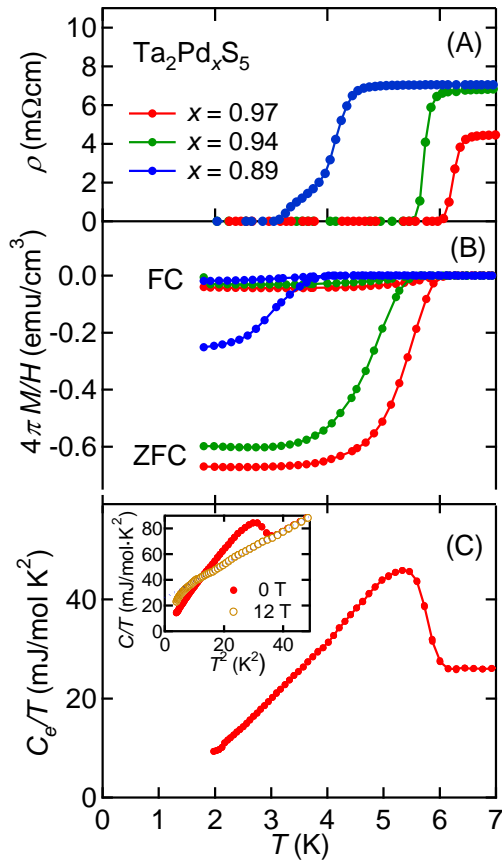


Figure 6-3: Superconducting transition in Ta₂Pd_xS₅ polycrystalline samples evidenced by (A) zero resistivity (B) Meissner effects and (C) electronic heat capacity divided by temperature. Ta₂Pd_{0.97}S₅ was used for heat capacity measurement and clear anomaly can be identified at 5.8 K, evidencing bulk superconductivity. The inset of (C) is the heat capacity divided by temperature taken under 1 T (red marks) and 12 T (yellow marks), respectively [49].

6. 3 H_{c2} beyond the Pauli limit

Fig. 6-4 (A) shows the superconducting transition of single crystalline $\text{Ta}_2\text{Pd}_{0.92}\text{S}_5$ ($T_c = 5.4$ K) under magnetic field. The $\mu_0 H_{c2}(T)$ is obtained from the midpoints of the resistive transition which are plotted in Fig. 6-4 (B). The slopes

$\left(\mu_0 \frac{dH_{c2}}{dT}\right)_{T=T_c}$ are calculated to be -8.5 T/K ($H \parallel b$ -axis) and -3.7 T/K ($H \perp b$ -axis),

respectively. The $\mu_0 H_{c2}$ at 0 K is calculated by using simplified Werthamer-Helfand-Hohenberg (WHH) formula [49],

$\mu_0 H_{c2}^*(0) = -0.698 \times \left(\mu_0 \frac{dH_{c2}}{dT}\right)_{T=T_c} \times T_c$, which gives the orbital limit $\mu_0 H_{c2}^*(T)$ to be 32

T ($H \parallel b$ -axis) and 14 T ($H \perp b$ -axis), respectively. The Ginzburg-Landau coherence length of superconductivity ξ_{GL} of each direction were therefore calculated to be $\xi_{\text{GL}} = 3.2$ nm ($H \parallel b$ -axis) and $\xi_{\text{GL}} = 4.8$ nm ($H \perp b$ -axis), respectively. Considering that the electronic resistivity at 10 K is as large as 300 m Ω cm, the electrons mean free path l_{tr} can be calculated to be ~ 0.6 nm along the b -axis. It is discovered that the electron mean free path is consistent with the distance between palladium deficiencies in $\text{Ta}_2\text{Pd}_{0.92}\text{S}_5$ crystals along the b -axis^{vi}. This indicates that palladium defects are the main electron scattering center. Since the calculated electron mean free path l_{tr} is even shorter than obtained GL coherence length ξ_{GL} , we argue that $\text{Ta}_2\text{Pd}_x\text{S}_5$ can be regarded as a dirty-limit superconductor.

^{vi} Since $\text{Ta}_2\text{Pd}_{0.92}\text{S}_5$ contains 0.32 palladium defects per one unit cell ($Z = 4$), the distance between palladium defects along the b -axis is calculated to be 0.9 nm, which is in good agreement with experimental data.

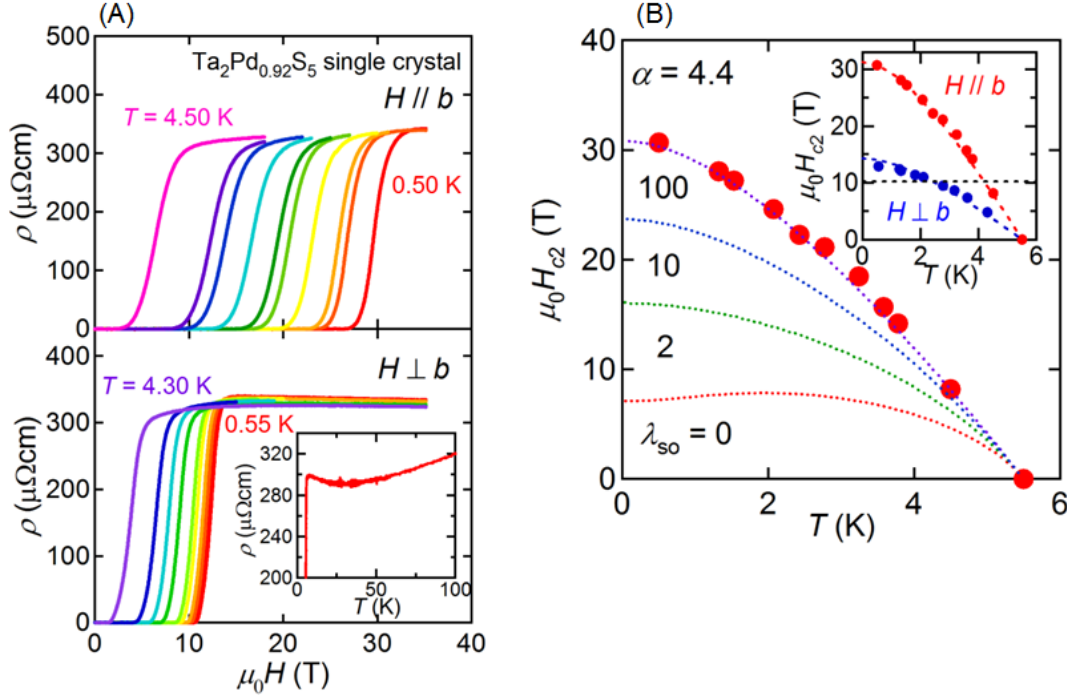


Figure 6-4: (A) Resistive superconducting transition of $\text{Ta}_2\text{Pd}_{0.92}\text{S}_5$ single crystal ($T_c = 5.4$ K) with applying magnetic fields parallel and perpendicular to the b -axis, i.e. quasi-one dimensional TaS_6 chains. (B) Temperature dependence of $\mu_0 H_{c2}$ with magnetic field applied parallel to the b -axis. The red solid circle is the experimental data points and dashed lines are the calculated $\mu_0 H_{c2}(T)$ based on WHH theory. The Maki parameter used in the calculation is $\alpha = 4.4$ and spin-orbit scattering parameter are $\lambda_{\text{SO}} = 0, 2, 10$ and 100 , respectively [49].

6. 4 Discussion of the chapter

The large orbital limit $\mu_0 H_{c2}^*(T)$, 32 T ($H \parallel b$ -axis), gives us an opportunity to challenge the Pauli limit. Except for the orbital limit, superconductivity can be destroyed by paramagnetic pair breaking effect when the paramagnetic energy $1/2 \chi_P H^2$ exceeds the superconducting condensation energy $1/2 D(\epsilon_F) \Delta^2$. Here χ_P is the magnitude of Pauli paramagnetism, $D(\epsilon_F)$ is the electronic density of state at Fermi level and Δ is the magnitude of superconducting gap, respectively. In a weak-coupling BCS superconductor, the Pauli limit can be expressed as $\mu_0 H_{\text{Pauli}} = 1.84 T_c$ [T], by employing $2\Delta = 3.52 k_B T_c$ and g -factor of free electron 2, which gives 10.2 T for the $\text{Ta}_2\text{Pd}_{0.92}\text{S}_5$ single crystals [51]. The Pauli limiting effect of $\mu_0 H_{c2}(T)$ has been observed in the spin-singlet superconductors including α -(ET) $_2\text{NH}_4(\text{SCN})_4$ [52] and iron-based superconductors [53]. Surprisingly, it is discovered that the measured $\mu_0 H_{c2}(T)$ of

Ta₂Pd_{0.92}S₅ at 0 K surpasses the Pauli limit as shown in Fig. 6-4 (B). The extrapolated $\mu_0 H_{c2}(0)$ is found to be 31 T ($H \parallel b$ -axis) and 14 T ($H \perp b$ -axis), respectively. The experimentally observed $\mu_0 H_{c2}(0)$ are consistent with calculated orbital limit, indicating that the Pauli paramagnetic effect is almost suppressed in the system.

There are several factors which could suppress paramagnetic pair breaking effect. First, in spin-triplet superconductors, such as (TMTSF)₂PF₆ [54], Sr₂RuO₄ [55] and URhGe [56], there should be no paramagnetic pair breaking effect since χ_P remains finite even in superconducting state. Second, the strong-coupling superconductivity would enhance Pauli limit since the superconducting gap is enhanced compared to BCS weak-coupling [57]. Furthermore, a reduced g -factor also can suppress the paramagnetic effect as discussed in URu₂Si₂ [58]. This effect could be pronounced in superconductors with heavy elements such as 5d transition metal. However, Ta₂Pd_xS₅ is discovered to be a BCS weak-coupling superconductor in dirty limit. This excludes the possibilities of spin-triplet and strong coupling scenario to explain the violation of Pauli limit. The reduced g -factor is neither the case. The magnetic susceptibility of the Ta₂Pd_xS₅ polycrystalline samples in the normal state is almost temperature independent, dominated by Pauli paramagnetism with $\chi_P = 3.8 \times 10^{-4}$ emu/mol. By subtracting the core diamagnetism which is obtained from the ionic values for tantalum, palladium and sulfur, the paramagnetic susceptibility is estimated to be $\chi_P = 6 \times 10^{-4}$ emu/mol. Combined with $\gamma = 27.6$ mJ/(mol K²), the Wilson ratio is evaluated to be 1.6, moderately enhanced compared with the free electron value of 1, and therefore pronounced reduction of g -factor is highly unlikely.

From the consideration above, we argue that the spin-orbit scattering, associated with the presence of heavy tantalum and palladium atoms, plays significant role to realize high $\mu_0 H_{c2}$ in the system. Spin-orbit scattering gives rise to remnant spin paramagnetic susceptibility even in the superconducting state, and therefore suppresses paramagnetic pair breaking effect. The effect can be described within the parameter $\lambda_{so} = 2\hbar/3\pi k_B T_c \tau_{so}$ where τ_{so} and λ_{so} demote a relaxation time and mean free path of spin-orbit scattering, respectively. With λ_{so} , $\mu_0 H_{c2}(T)$ is determined to be

$$\ln\left(\frac{1}{t}\right) = \sum_{\nu=-\infty}^{\infty} \left\{ \frac{1}{|2\nu+1|} - \left[|2\nu+1| + \frac{\bar{h}}{t} + \frac{(\alpha\bar{h}/t)}{|2\nu+1| + (\bar{h} + \lambda_{so})/t} \right]^{-1} \right\} \quad (5-1)$$

where t and \bar{h} is the reduced temperature and field, respectively which can be expressed as $t = T/T_c$ and $\bar{h} = 0.281 H_{c2}(T)/H_{c2}^*(0)$. $\alpha = \sqrt{2} H_{c2}^*(0)/H_p$ is the Maki parameter, a ratio of the orbital limiting critical field and the Pauli limiting field,

providing a measure of the paramagnetic effect. In $\text{Ta}_2\text{Pd}_{0.92}\text{S}_5$, α is estimated to be 4.4 ($\mu_0 H_{c2}^*(0) = 32$ T and $\mu_0 H_P = 10.2$ T). By tuning λ_{so} as a fitting parameter, we obtain large $\lambda_{\text{so}} \sim 100$ to reproduce $\mu_0 H_{c2}(T)$. The large λ_{so} simply reflects that $\mu_0 H_{c2}(T)$ behaves as if there were no Pauli paramagnetic pair breaking.

Considering that calculated carrier density is the order of 10^{22} cm^{-3} , the spin-orbit scattering length l_{SO} is estimated to be ~ 1 nm. This implies that spin-orbit scattering is as strong as transport scattering by palladium defects which gives $l_{\text{tr}} \sim 0.6$ nm. The effect of spin-orbit scattering is profound when heavy mass impurities are present. The suppression of paramagnetic pair breaking due to heavy mass impurities were discussed in a variety of superconductors partly motivated by the possibility of enhancing $\mu_0 H_{c2}(T)$. In the case of $\text{Ta}_2\text{Pd}_x\text{S}_5$, palladium deficiencies, the main cause of transport scattering, are not heavy mass impurities. Strong spin-orbit coupling is expected for $5d$ Ta and $4d$ Pd. However, those form a periodic lattice and do not contribute as spin-orbit scatterers. We argue that palladium deficiencies embedded in the lattice of heavy elements may act analogous to heavy elements in a lattice of light elements. Palladium deficiencies in this case scatter electrons and holes in $5d$ and $4d$ bands where the spins are coherently and strongly entangled with the momentum. They could be strong spin-orbit scatterers as well as transport scatterers. In the dirty limit, such spin-orbit scattering should be maximized [48].

6.5 Summary of the chapter

In summary, we discovered a new superconductor $\text{Ta}_2\text{Pd}_x\text{S}_5$ with $T_c \sim 6$ K, evidenced by transport, magnetic susceptibility and thermodynamic properties. The electron mean free path l_{tr} along the b -axis is estimated to be as long as ~ 0.5 nm, which is much shorter than its BCS coherence length. This indicates that $\text{Ta}_2\text{Pd}_x\text{S}_5$ is a dirty limit superconductor and therefore orbital limit can be enhanced. Combining with thermodynamic property of electronic system, it is concluded that $\text{Ta}_2\text{Pd}_x\text{S}_5$ hosts a weak-coupling BCS superconductor. Intriguingly, the $\mu_0 H_{c2}$ of $\text{Ta}_2\text{Pd}_x\text{S}_5$ is measured to be 31 T along the b -axis and violates Pauli limit by a factor of three. Since $\text{Ta}_2\text{Pd}_x\text{S}_5$ is a weak-coupling BCS superconductor, spin-orbit scattering should play significant roles for suppressing paramagnetic pair breaking effect. We argue that spin-orbit scattering induced by palladium deficiencies act as ‘spin-orbit vacancies’ embedded in the periodic lattice of heavy tantalum and palladium.

Chapter 7 Discussion

Ta_2NiSe_5 has several unique properties among excitonic insulator candidate materials. First and foremost, it is the only direct gap ($q = 0$) semiconductor in this group of materials. The formation of a small direct gap is possible since the normal state valence and conduction bands belong to different irreducible representations of the crystal symmetry [41-43]. This excludes the possibility of simple band hybridization in the high temperature orthorhombic phase [43]. A direct consequence of this unique situation is the absence of a finite- q lattice distortion and the significant changes in the phonon excitation spectrum observed in other candidate systems. Instead, the transition is accompanied by a small $q = 0$ lattice distortion which achieves the necessary lowering of the symmetry from an orthorhombic to a monoclinic unit cell. In this chapter, we will summarize the experimental data obtained so far and discuss why an excitonic insulator state is stabilized in Ta_2NiSe_5 .

7. 1 Is Ta_2NiSe_5 an excitonic insulator?

In an excitonic insulator, an excitonic gap associated with exciton condensation emerges in both conduction and valence bands below T_c [8]. This should give rise to a significant change in the electronic heat capacity since the part of condensed carriers lose their entropy. While the gap formation and large entropy change are the generic features of an excitonic insulator, neither of them has been reported in the previous studies. Furthermore, the characteristic phase diagram and the estimation of exciton binding energy should be compelling experimental evidences for an excitonic insulator phase. In order to address these issues and check the consistency with excitonic insulator scenario, we focused on basic physical properties of pure and chemical substituted Ta_2NiSe_5 , including transport, optical and thermodynamic properties.

7. 1. 1 Gap opening below T_c

A clear gap formation is one of the most highlighted properties in an excitonic insulator. In order to identify the presence of the excitonic gap, we have investigated the transport and optical properties of Ta_2NiSe_5 . Our transport measurements show that the high temperature phase of pure Ta_2NiSe_5 is a close-to-zero gap system, and it undergoes a semiconductor-to-insulator transition at 326 K, implying that a gap opens in the Fermi

level. A clear gap formation was directly evidenced by our optical conductivity measurements. At 10 K, the gap become significant at 0.3 eV point and the peak point is located at 0.4 eV, indicating that the magnitude of the gap is in the range of 0.3 – 0.4 eV (see Fig. 4-4). Since the activation energy above T_c is considerably small, it should predominantly reflect the magnitude of the excitonic gap 2Δ , indicating that the phase transition is in the strong coupling regime with $2\Delta/k_B T_c = 13 - 15$. Here the gap in the valence band is reported to be 0.17 eV from ARPES technique [11,44]. Therefore, at least 0.13 eV gap formation can be expected in the conduction band. Intriguingly, a pseudo-gap feature also can be identified from our high temperature resistivity measurements. The Arrhenius plot of pure Ta_2NiSe_5 is found to be temperature dependent while the activation energy of pure Ta_2NiS_5 is temperature invariant (see the Fig. 4-3 (B)). The pseudo-gap feature, associated with exciton fluctuation, is consistent with strong coupling, i.e. non-BCS type, transition as discussed theoretically [10,11].

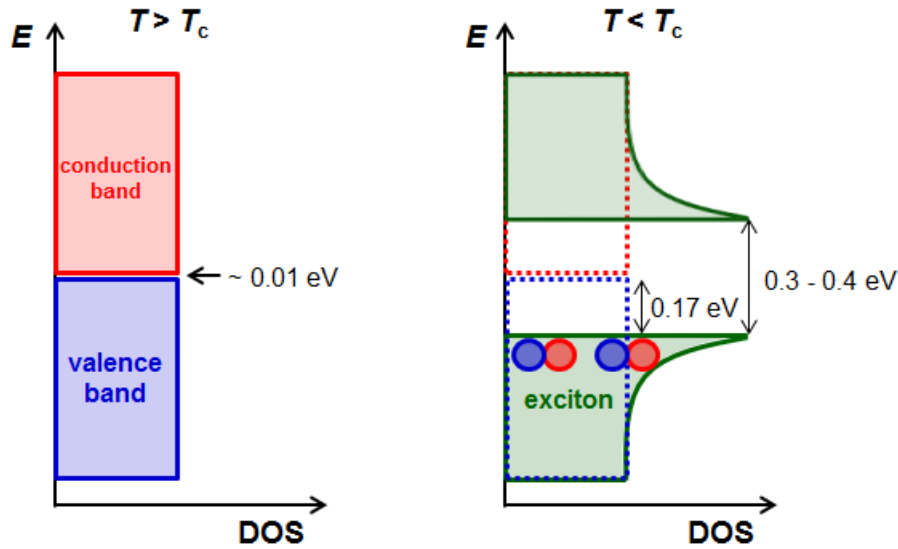


Figure 7-1: The schematic picture of electronic density of state in Ta_2NiSe_5 . In the high temperature phase, the activation energy is estimated to be 0.01 eV while a clear gap as large as 0.3 - 0.4 eV opens in below T_c . The gap in the valence band is reported to be 0.17 eV from the previous spectroscopic study [11,44].

7. 1. 2 The evidence of exciton condensation

An excitonic gap formation should give rise to a significant entropy change in the electronic system. In order to check the consistency of the exciton condensation, we have investigated thermodynamic properties of Ta_2NiSe_5 . A pronounced heat capacity anomaly can be identified at T_c , which gives the entropy change of the phase transition

to be $\Delta S \sim 0.6 \text{ J}/(\text{mol K})$ (see Fig. 4-5). This corresponds to approximately 7 % of gas constant and it is clearly too large to be accounted for only as contribution from the lattice degree of freedom. Here it is considered that the carriers in the range of $k_B T$ ($T = 326 \text{ K}$ in Ta_2NiSe_5) from Fermi level hold $3k_B$ of entropy above T_c (see Fig. 7-1 (A)). The electronic density of state of Ta_2NiSe_5 valence band is reported to be the order of 1 state/eV [43]. Therefore, the total entropy change is well reproducible by assuming that those carriers, in the $k_B T$ range from Fermi level, lose their entropy due to exciton condensation.

7. 1. 3 The relevant energy scale of Ta_2NiSe_5

In an excitonic insulator, exciton binding energy E_B should exceed the magnitude of the activation energy of the material and become comparable to the magnitude of excitonic gap 2Δ . Here the E_B can be expressed as following equation,

$$E_B = \frac{13.6\mu}{m_0\varepsilon^2} (\text{eV}) \quad (7-1)$$

where μ is the reduced exciton mass which is given by $1/\mu = 1/m_e + 1/m_h$. m_e and m_h are the effective mass of electron and hole, respectively. m_0 is the bare electron mass and ε is the relevant permittivity. Based on the published band calculations, we can estimate the reduced mass μ to be of the order of $1m_0$ [43]. Fig. 7-2 (A) shows the relevant permittivity as a function of photon energy which is taken at 350 K and 10 K, respectively. Here, $\varepsilon_\infty = 8$ should be used for the exciton binding energy calculation [7]. We have employed permittivity of 1 eV point since the value is sufficiently larger than the magnitude of the excitonic gap $2\Delta^{\text{vii}}$. This allows for a rough estimation of exciton binding energy to be $E_B \sim 0.19 \text{ eV}$.

Crucially, the calculated binding energy is clearly larger than the magnitude of activation energy, 0.01 eV, and therefore the electron-hole Coulomb interaction should be strong enough to give rise to an excitonic insulator transition [8]. Furthermore, the estimated binding energy is found to comparable to the excitonic gap $2\Delta = 0.3 - 0.4 \text{ eV}$ observed by our optical conductivity measurements as summarized in Fig. 7-2 (C) [11,44].

^{vii} The relevant permittivity ε_0 and ε_∞ were measured by Prof. B. Keimer's group to be 10 and 8, respectively at 350 K.

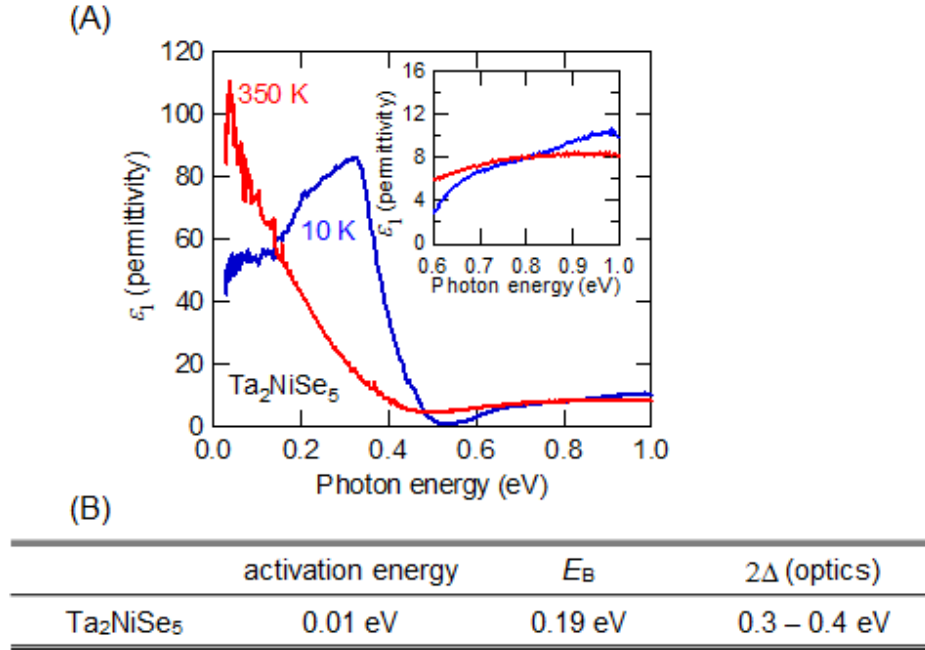


Figure 7-2: (A) The relevant permittivity of Ta₂NiSe₅ as a function of photon energy taken by using spectroscopic ellipsometry at 10 K and 350 K. The permittivity at 1 eV point is used to calculate exciton binding energy. (B) The relevant energy scale of Ta₂NiSe₅. The magnitude of excitonic gap obtained from spectroscopic measurement shows good agreement with calculated exciton binding energy.

7. 1. 4 The electronic phase diagram

The electronic phase diagram as a function of activation energy is one of the outstanding characters of an excitonic insulator. Since the Ta₂NiSe₅ is considered to locate at optimal point of the phase transition, we have employed pressure effect to investigate the semi-metallic region of the phase diagram. By using activation energy at 300 K, we could estimate the pressure effect to be 0.06 eV/GPa in pure Ta₂NiSe₅ (see Fig. 5-4 (B)). Since the activation energy of Ta₂NiSe₅ is as large as 0.01 eV, the pressure range up to 3 GPa is sufficiently large to drive Ta₂NiSe₅ to be a semi-metallic state as summarized in Fig. 7-3. Indeed, we observed that electronic resistivity of Ta₂NiSe₅ become more conductive as pressure increases with a systematic suppression of T_c , indicating that increasing carrier density screens electron-hole Coulomb interaction. A 1st order transition at around 3 GPa can be identified. We argue that the pressure induced phase transition is not related to the excitonic insulator physics discussed in the thesis, but structural instability since all chemical substituted Ta₂NiSe₅, which has

different activation energy and T_c , undergoes the 1st order transition at same pressure range.

Sulfur substitution, on the other hands, is used to extend the range of activation energy towards the semiconductor side of the phase diagram. Again, we confirmed a systematic suppression of T_c with enhancing activation energy as expected within the excitonic insulator scenario. Intriguingly, it is discovered that the phase transition is completely suppressed when the magnitude of the activation energy become as large as 0.12 eV, which is even smaller than the calculated binding energy, 0.19 eV. It is considered that sulfur doping effect not only changes the band overlap but also induces impurity states which can significantly influence the carrier concentration, and therefore electron-hole Coulomb interaction can be screened. However, we argue that the electronic phase diagram is still consistent with excitonic insulator scenario since enhancement of T_c can be seen by applying pressure to sulfur substituted Ta_2NiSe_5 . The pressure effect of $Ta_2Ni(Se_{0.84}S_{0.16})_5$ and $Ta_2Ni(Se_{0.68}S_{0.32})_5$ are also illustrated in Fig. 7-3. The pressure effect of sulfur substituted Ta_2NiSe_5 were calculated to be 0.03 eV/GPa according to the activation energy obtained at 300 K (see Fig. 5-4). Since the activation energy of $Ta_2Ni(Se_{0.84}S_{0.16})_5$ and $Ta_2Ni(Se_{0.68}S_{0.32})_5$ are estimated to be 0.03 eV and 0.04 eV under ambient pressure, respectively, the activation energy under pressure can be calculated by subtracting 0.03 eV/GPa which is illustrated in Fig. 7-3.

Overall, we discovered that both increasing and decreasing activation energy suppresses T_c systematically. Since Ta_2NiSe_5 locates at the optical point of the phase diagram, the pressure and sulfur substitution drive the system to be semi-metallic and semiconducting state, respectively. The obtained experimental data is highly consistent with the electronic phase diagram predicted theoretically.

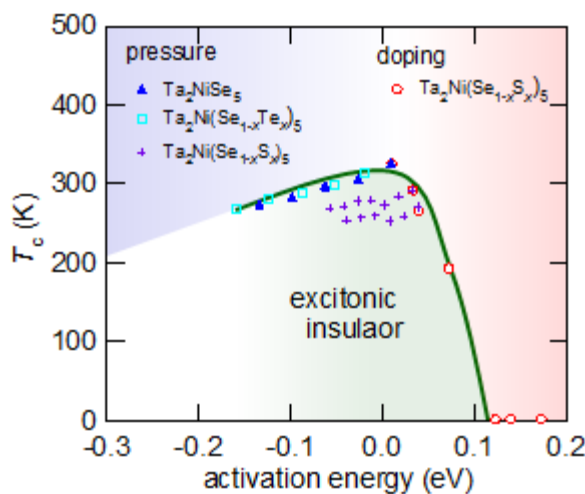


Figure 7-3: The electronic phase diagram of Ta_2NiSe_5 as a function of activation energy. The red point denotes T_c of sulfur substituted Ta_2NiSe_5 . The blue, green and purple points represent T_c of pure, S 16 % and S 32 % doped Ta_2NiSe_5 under pressure, respectively. The activation energy was calculated by subtracting estimated pressure effect.

7. 1. 5 Supporting evidences of the excitonic insulator transition

The presence of an excitonic insulator state in Ta_2NiSe_5 is furthermore supported by the isotropic in-plane resistivity below T_c . The reported band calculation expects the anisotropic in-plane resistivity since the effective mass along the X- Γ -X and Z- Γ -Z direction is different. The electronic resistivity is found to be more conductive when the electronic current is applied along the a -axis, however, more isotropic in-plane conductivity can be identified in the low temperature phase. We argue that it can attribute to electron-hole hybridization between TaSe_6 and NiSe_4 chains. Fig. 7-4 shows the schematic crystal and the electronic structure (molecular orbitals) of Ta_2NiSe_5 layer above and below T_c . Since Ta_2NiSe_5 is a direct gap system, the phase transition is accompanied by a small and uniform lattice distortion which lowers the crystal symmetry from an orthorhombic to a monoclinic system [42]. At $T > T_c$, the system is orthorhombic and the hybridization between TaSe_6 chains and NiSe_4 chains are forbidden due to the crystal symmetry. In the low temperature phase, small lattice distortion appears and the angle β become larger than original angle, 90 degrees, resulting in the monoclinic structure. In the monoclinic crystal symmetry, there is finite overlap between TaSe_6 and NiSe_4 chains and therefore the system can form hybridization gap in the conduction and valence band as shown in Fig. 7-4. Consequently, the hybridization between the chains gives rise to more isotropic

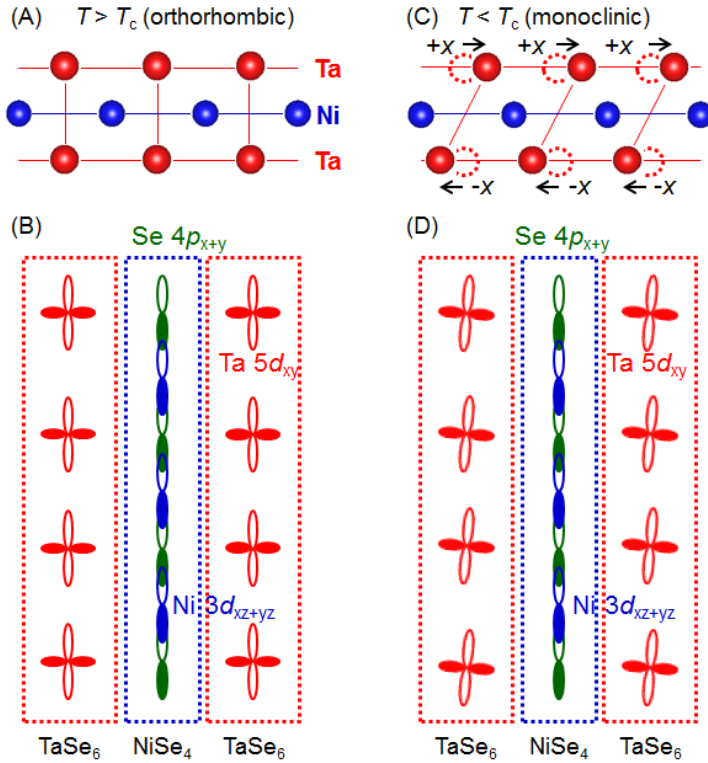


Figure 7-4: (A) Schematic crystal structure of and (B) molecular orbitals of Ta_2NiSe_5 in the orthorhombic phase. The hybridization between TaSe_6 and NiSe_4 chains are forbidden by the crystal symmetry. (C) Schematic crystal structure and (D) molecular orbitals of Ta_2NiSe_5 in the monoclinic phase. Finite coupling between TaSe_6 and NiSe_4 chains can be expected [43].

electronic conductivity, consistent with our in-plane electronic resistivity measurements as shown in Fig. 4-1 (B)^{viii} .

The lattice distortion, show in Fig. 7-4, is small in Ta₂NiSe₅ compared to 1T-TiSe₂ and TmSe_{0.45}Te_{0.55}, however, the effect of electron-lattice coupling still may affect the phase transition in some degree in an excitonic insulator transition. T. Kaneko et al. calculated the effect of lattice deformation and electron-phonon coupling in Ta₂NiSe₅ by using band structure calculation and mean-field analysis of the derived three chains Hubbard model with phonon degree of freedom [43]. Fig. 7-4 (C) and Fig. 7-5 show the schematic deformation of lattice and calculated phase diagram of Ta₂NiSe₅ as functions of λ and V . Here λ is defined as following equation,

$$\lambda = \frac{g^2}{\omega} = \frac{\gamma^2}{2K} \quad (7-1)$$

where g and ω are the electron-phonon coupling and phonon frequency, respectively, and V is the inter-chain electron-hole Coulomb interaction. Here ω and g are defined to be $\omega = (K/M)^{1/2}$ and $g = \gamma/(2\omega M)^{1/2}$ where K is the spring constant of lattice, M is the atomic mass and γ is the strength of hybridization between conduction and valence band, respectively [43]. It is noteworthy that even if λ is zero, system can undergo a phase transition with help of electron-hole coupling. The magnitude of λ , i.e. electron-phonon coupling, is calculated by using real parameter of Ta₂NiSe₅. Here the structural distortion of Ta₂NiSe₅ is reported to be $\Delta\beta = 0.5 - 1.0$ degrees [41,42]. This results in atomic displacement of $x = 0.02 - 0.04$ Å below T_c as depicted in Fig. 7-4 (C). The effect of lattice distortion is estimated by numerical calculations. By assuming atomic displacement of $x = 0.02 - 0.04$ Å, it is calculated that the gap as large as $|\delta| = 0.02 - 0.04$ eV opens without electron-hole coupling. Since the strength of hybridization between conduction and valence band γ is defined as $\gamma = |\delta|/x$, it is calculated to be $\gamma = 1$ eV/Å. Here the spring constant is roughly calculated to be $K = 10 - 30$ eV/Å², giving the electron-phonon coupling to be $\lambda = \gamma^2/2K = 0.02 - 0.05$ eV [43]. The reported value of λ and $|\delta|$ is found to be smaller than the critical value $\lambda_c = 0.12$ eV and the gap observed in Ta₂NiSe₅ valence band $\Delta \sim 0.17$ eV, respectively, implying that electron-hole coupling should play more significant role for the phase transition in Ta₂NiSe₅. It is in strong contrast to a conventional CDW state which undergoes a phase transition with help of a finite- q lattice distortion associated with Fermi surface nesting.

^{viii} The hybridization between TaSe₆ and NiSe₄ chains give rise to finite band dispersion along the Z-Γ-Z direction.

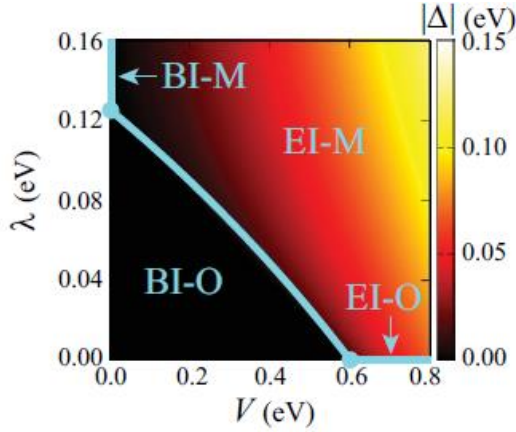


Figure 7-5: (A) Phase diagram of excitonic gap Δ in Ta_2NiSe_5 as a function of electron-phonon coupling λ and inter-chain electron-hole coupling V [43].

In conclusion, we have demonstrated that an excitonic insulator transition manifest itself in a close-to-zero gap semiconductor Ta_2NiSe_5 below 326 K. We could successfully identify the presence of an excitonic gap and large entropy change inherent in an excitonic insulator. The band gap dependent T_c is furthermore consistent with excitonic insulator scenario. The electronic phase diagram is found to emerge in both semiconductor and semi-metallic region, indicating that the T_c of Ta_2NiSe_5 is sensitive to the magnitude of activation energy. The large electron-hole Coulomb interaction is the highlighted character of Ta_2NiSe_5 . The exciton binding energy of Ta_2NiSe_5 is roughly calculated to be $E_B = 0.19$ eV, which is sufficiently larger than the band gap, 0.01 eV. Furthermore, the calculated E_B is found to be comparable to the magnitude of excitonic gap 2Δ , consistent with excitonic insulator scenario. While the effect of band hybridization cannot be excluded to explain the origin of the phase transition in Ta_2NiSe_5 , such strong electron-hole interaction is considered to be a key driving force of the phase transition in Ta_2NiSe_5 .

7. 2 Uniqueness of Ta₂NiSe₅ as an excitonic insulator

Ta₂NiSe₅ has several unique characters as an excitonic insulator. First, a ‘clean’ excitonic insulator transition should be a highlighted character of Ta₂NiSe₅. While a clear gap formation, large entropy change associated with exciton condensation and the electronic phase diagram are the generic features of an excitonic insulator, we are aware that these only can be identified in Ta₂NiSe₅ in the group of materials, including TmSe_{0.45}Te_{0.55} and 1*T*-TiSe₂. While a characteristic phase diagram can be identified in TmSe_{0.45}Te_{0.55}, none of the literatures has reported the presence of a hybridization gap in the system [21-23]. Furthermore, the thermodynamic evidences for exciton condensation are obscured due to magnetic momentum of Tm ion [37]. It is reported that the heat capacity anomaly of TmSe_{0.45}Te_{0.55} observed under high pressure mainly originate from localized spin momentum of Tm ion which is not related to exciton condensation [37]. The case of 1*T*-TiSe₂ is furthermore complicated since the phase transition is accompanied by a strong lattice distortion. It is discovered that both conduction and valence band become more stable in energy below T_c associated with modification of crystal field [39]. This complicates the electronic structure of 1*T*-TiSe₂ and therefore band Jahn-Teller effect has also been invoked as a driving force of the phase transition. A heat capacity anomaly can be identified at T_c in 1*T*-TiSe₂, giving entropy change of the phase transition to be $\Delta S \sim 0.1$ J/(mol K). However, since the gap formation in the valence band is $\Delta \sim 0.1$ eV in 1*T*-TiSe₂, the estimated entropy change is seems to be too small to explain exciton condensation, which is highly unlikely for an excitonic insulator transition^{ix}. The observation of physical properties inherent in an excitonic insulator is possible in Ta₂NiSe₅ since it has a direct gap band structure ($\mathbf{q} = 0$) and does not have localized magnetic momentum. Therefore the effect of lattice distortion and magnetic momentum is absent in the material, which manifest the ‘cleanest’ excitonic insulator transition.

Second, a non-BCS like transition with $2\Delta/k_B T_c = 13 - 15$ is also an outstanding character. The pseudo-gap feature observed in our high temperature measurement is consistent with such strong coupling transition. Intriguingly, precursor upturn in E_ρ vs T plot survives in the sulfur doped Ta₂NiSe₅ while it vanishes very quickly by applying pressure (see Fig. 5-4). We argue that the pseudo-gap formation is suppressed in the semi-metallic region due to the increasing carrier density which should screens Coulomb interaction between electron and hole, resulting in more BCS-like excitonic

^{ix} The entropy change as large as $\Delta S \sim 0.4$ J/(mol K) is expected within the excitonic insulator scenario in 1*T*-TiSe₂.

insulator transition. The experimental data implies that BCS-BEC crossover manifest itself in the phase diagram of Ta₂NiSe₅ (see Fig. 7-3). While several theoretical studies expect a BCS-BES crossover in an excitonic insulator transition, none of the materials besides Ta₂NiSe₅ have been reported to the case experimentally. Therefore, the excitonic insulator transition in Ta₂NiSe₅ can be a solid state platform to explore high- T_c BCS-BEC crossover.

Finally, we discuss the characteristic band structure of Ta₂NiSe₅ which realizes large exciton binding energy. Needless to say, excitonic insulator state is only possible when the exciton binding energy exceeds the magnitude of band gap of materials. The magnitude of exciton binding energy E_B and band gap E_G are the basic parameter of semiconductors and therefore has been studied for a long time. Table 7-1 shows the reported band gap E_G , reduced mass of carriers, μ , relevant permittivity, ϵ , and exciton binding energy E_B of semiconductors. It is clearly seen that magnitude of the band gap E_G is larger than exciton binding energy E_B in most of materials. We argue that the magnitude of exciton binding energy E_B is reduced due to relative light effective mass of carriers. In most of semiconductors, including oxides and III-V type semiconductors, valence and conduction bands are composed of p - or s -orbitals. Fig. 7-6 shows the band structure of ZnO by deputy [63]. It is reported that valence and conduction bands are composed by O $2p$ and Zn $3d$ orbitals while Zn $4s$ orbitals dominate its conduction band, respectively. The p or s characters of valence and conduction bands are universal among semiconductors and effective mass of carriers tend to be lighter than the carriers in d -orbitals. Here exciton binding energy E_B is determined by reduced mass, μ . It is noteworthy that reduced mass μ is dominated by ‘lighter’ carrier and even heavy effective electron (or hole) mass is realized in a material, the lighter hole (or electron) significantly suppresses the magnitude of μ . Therefore both heavy electron and hole are essential for realizing large exciton binding energy. In Ta₂NiSe₅, it is characteristic that both of conduction and valence bands are composed by d -orbitals, and therefore relative large μ is realized, resulting in large exciton binding energy E_B . This is in strong contrast to the other semiconductors as listed in Table 7-1. We argue that large exciton binding energy is realized in Ta₂NiSe₅ due to the strong d -character of both conduction and valence bands.

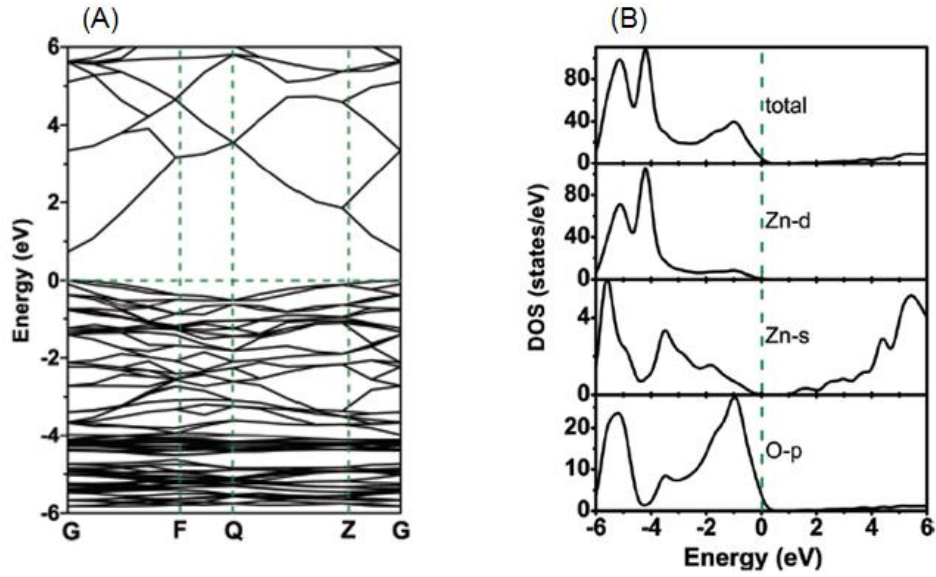


Figure 7-6: (A) Calculated band structure and (B) electronic density of state of ZnO. The Fermi level is defined to be zero as guided by green dashed line [63].

Table 7-1: The magnitude of band gap E_G , reduces mass μ , dielectric constant ε and exciton binding energy E_B of semiconductors reported in the literatures. m_0 denotes free electron mass [60-64].

materials	E_G (eV)	μ/m_0	ε	E_B (meV)
Si	1.11	-	-	14.7
Ge	0.67	-	-	4.15
GaAs	1.43	0.067	13	4.2
GaP	2.26	-	-	3.5
GaN	3.4	0.16	9.5	24
InSb	0.24	0.015	16	0.8
CdS	2.58	0.15	5.7	63
CdSe	1.73	0.13	10	18
KCl	~9	-	-	400
KBr	~8	-	-	400
Cu ₂ O	2.17	<0.35	7	9.72
SnO ₂	3.6	0.28	14	19.4
ZnO	3.2	0.19	8.5	60
ZnS	3.6	0.2	8.3	40
ZnSe	2.7	0.14	9.1	22
Ta₂NiSe₅	0.01	1	8	190

7.3 Future perspectives

The direct gap band structure of Ta_2NiSe_5 gives rise to a very clean excitonic insulator transition. This motivates us to furthermore investigate the physical properties of Ta_2NiSe_5 including NMR and ultrasonic attenuation measurements. They are the powerful experimental techniques to identify the coherence factor of materials, especially in a superconducting transition. In an excitonic insulator, it has been theoretically discussed that the relaxation of NMR has anomalous temperature dependence associated with coherence factors which is analogous to the case of superconductivity [64]. Therefore it could be a prospective perspective to furthermore identify the excitonic insulator state in Ta_2NiSe_5 by detecting ultrasonic absorption and relaxation time ($1/T_1$) as a function of temperature.

The large exciton binding energy realized in Ta_2NiSe_5 also gives important suggestions for further exploring excitonic insulator candidate. It is essential to realize heavy effective mass of both electron and hole in an excitonic insulator. In order to realize d -character in both conduction and valence band, it is useful to employ transition metal oxides or chalcogenides which include IV~VI and IX~XII family transition metals. Fig. 7-7 shows the energy level of 3 - 5d orbitals in transition metals. It is clearly seen that the energy level of IV family is the highest while it becomes lower in IX ~ XII transition metals due to increased core proton. The energy difference between the transition metals give rise to the separation of each d -orbital in energy in the momentum space and realizes the situation that both conduction and valence band are composed of d -orbitals as represented in Ta_2NiSe_5 and Ta_2PdS_5 . We argue that these transition metal oxides or chalcogenides provides prospective possibilities to discover new excitonic insulator.

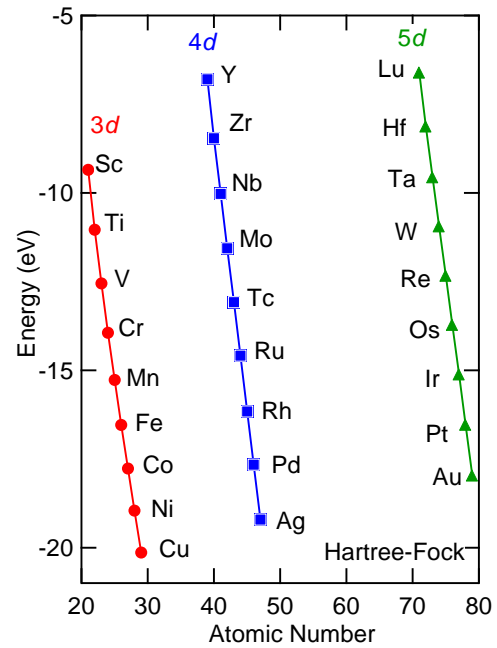


Figure 7-7: Orbital energy level of 3d, 4d and 5d transition metals calculated by using Hartree-Fock approximation. In the category of 3d, 4d and 5d transition metals, the energy level of d -orbitals are lowered as atomic number increases.

Chapter 8 Summary

Excitonic insulator is a strong electron-hole coupling driven phase, associated with exciton condensation, which is discussed to manifest itself in the semiconductor/semi-metal boundary. While the possibilities of excitonic insulator transition have been discussed in $\text{TmSe}_{0.45}\text{Te}_{0.55}$ and $1T\text{-TiSe}_2$, excitonic insulator state have yet been identified in those materials. In such indirect gap systems, the excitonic insulator transition is accompanied by a finite- q lattice distortion and it obscures excitonic gap formation and entropy change of the phase transition. In order to avoid the effect of such lattice distortion, we focused on newly discovered excitonic insulator candidate material Ta_2NiSe_5 which undergoes a semiconductor-to-insulator transition at 326 K. In this thesis, we have investigated transport, optical and thermodynamic properties of pure, sulfur and tellurium substituted Ta_2NiSe_5 and discovered that the phase transition is highly consistent with excitonic insulator scenario. We argue that the phase transition in Ta_2NiSe_5 is driven by a sufficiently strong electron-hole coupling.

In chapter 4, we have demonstrated the presence of an excitonic gap and large entropy change associated with exciton condensation inherent in an excitonic insulator. Ta_2NiSe_5 is discovered to be a close-to-zero gap semiconductor and an excitonic gap as large as $2\Delta = 0.3 - 0.4$ eV is identified from our optical conductivity measurement. The presence of an excitonic gap is furthermore evidenced by heat capacity measurements. We clearly observed an anomaly at T_c , giving entropy change of the phase transition to be $\Delta S \sim 0.6$ J/(mol K). It is discovered that the calculated entropy change can satisfactorily be interpreted by assuming that the carriers, in the $k_B T$ range from Fermi level, lose their entropy due to exciton condensation which is consistent with excitonic insulator transition.

In chapter 5, we have investigated the electronic phase diagram of Ta_2NiSe_5 as a function of band gap E_G which is one of the key experimental evidences for an excitonic insulator. The magnitude of band gap of Ta_2NiSe_5 is successfully controlled by using hydrostatic pressure and sulfur substitution which drive the system to be both more metallic and insulating, respectively. We discovered that T_c of Ta_2NiSe_5 is systematically suppressed with increasing and decreasing band gap E_G . Since Ta_2NiSe_5 is located at optical point of an excitonic insulator transition, the obtained electronic phase diagram is in good agreement with excitonic insulator scenario. Intriguingly, it is discovered that precursor upturn in E_ρ vs T plot associated with pseudo-gap formation persist in sulfur substituted system while it diminishes very quickly by applying pressure. Since electron-hole Coulomb interaction can be screened by increasing carrier

density, BCS-BES crossover expected in an excitonic insulator transition, is implied in the system.

The discovery of a new superconductor $\text{Ta}_2\text{Pd}_x\text{S}_5$ is reported in chapter 6. While the relationship between the excitonic insulator scenario in $\text{Ta}_2\text{Pd}_x\text{S}_5$ is unclear, it shows very high H_{c2} even beyond Pauli limit. We discovered that $\text{Ta}_2\text{Pd}_x\text{S}_5$ is a BCS weak coupling superconductor and large orbital limit is realized by a short electron mean free path, associated with palladium defects. Since $\text{Ta}_2\text{Pd}_x\text{S}_5$ is a weak-coupling BCS superconductor, spin-orbit scattering should play significant roles for suppressing paramagnetic pair breaking effect. We argue that spin-orbit scattering induced by palladium deficiencies act as ‘spin-orbit vacancies’ embedded in the periodic lattice of heavy tantalum and palladium.

Ta_2NiSe_5 has several unique properties as an excitonic insulator. First of all, it is the only direct gap material which undergoes an excitonic insulator transition without strong lattice distortion as discussed in $1T\text{-TiSe}_2$. Such clean transition get rid of the effect of electron-lattice coupling which allows us to identify the presence of hybridization gap, large entropy change and characteristic phase diagram which are inherent in an excitonic insulator. Second, an anomalously large exciton binding energy is realized in Ta_2NiSe_5 . The calculated value is large compared to well-studied semiconductor, including ZnO. We argue that an excitonic insulator state is stabilized by such large electron-hole Coulomb interaction enhanced by relative heavy carriers associated d -characters of conduction and valence band. Finally, the possibility of BCS-BEC crossover is first implied experimentally in the group of materials. Since the T_c of Ta_2NiSe_5 is much higher than that of cold atoms, Ta_2NiSe_5 can be an ideal solid state platform for high- T_c BCS-BEC crossover.

Appendix

Electronic resistivity measurement

The low temperature resistivities (1.8 K – 400 K) were measured by using PPMS (Quantum Design), and handmade measurement device was used for high temperature resistivity measurements (350 – 550 K). When the uniform electronic current is applied, the electronic resistivity ρ can be expressed by the following equation (Ohm's law):

$$\rho = \frac{V}{I} \frac{S}{L} \quad (\text{A-1})$$

where V is the voltage depression, L denotes the length between the electrode and S represents section area. The electronic resistivity measurements were measured by four-probe method in our study as illustrated in the Fig. A-1. Four-probe method is an electronic resistivity measurement which uses separate electrode pairs of current source and voltage meter. The separation of current and voltage electrodes eliminates the cable and contact resistance from the measurement. By using Kirchhoff's laws, the voltage depression V can be expressed by following equations,

$$\frac{V}{I} = R_{\text{sample}} - (R_{\text{cable}} + R_{\text{contact}} + R_{\text{sample}}) \frac{I_V}{I} \quad (\text{A-2})$$

$$\frac{I_V}{I} = \frac{R_{\text{sample}}}{R_{\text{cable}} + R_{\text{contact}} + R_{\text{sample}} + R_{\text{voltmeter}}} \quad (\text{A-3})$$

where R_{sample} , R_{cable} , $R_{\text{voltmeter}}$ and R_{contact} are the electronic resistivity of sample, cable, voltmeter and contact resistance, respectively. I is the applied current and I_V is the current along the voltmeter. Since the $R_{\text{voltmeter}}$ is assumed to be much larger than R_{sample} , I_V/I is close to zero and gives accurate R_{sample} from the measurement.

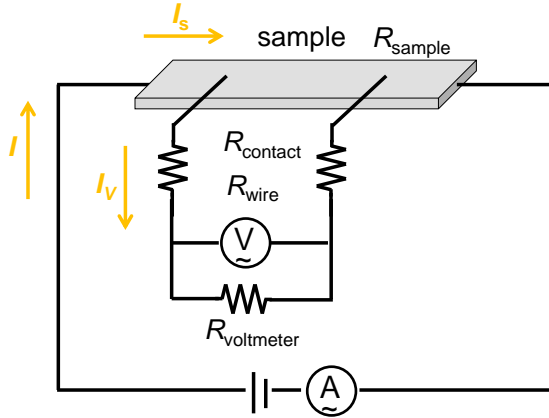


Figure A-1: Schematic picture of four probe method. R_{sample} , R_{contact} and R_{wire} denote electronic resistance of sample, contact and wire, respectively.

Heat capacity measurement

The heat capacity of Ta_2NiSe_5 was measured by using PPMS (Quantum Design) with the temperature range of 2 K – 400 K. The sample platform is composed by thermometer and heater which is connected with the thermal bath (puck frame) by the supporting wires as illustrated in Fig. A-2. Relaxation time method is employed to measure the heat capacity. Here we assume that the sample and sample platform are in good thermal contact with each other at same temperature during the measurement. When a constant heat power is provided into the system, the temperature T of the platform as a function of time t obeys the following equation

$$C_{\text{total}} \frac{dT}{dt} = Q(t) - \kappa(T - T_0) \quad (\text{A-4})$$

where C_{total} is the total heat capacity of the sample and sample platform, κ is the thermal conductance of the supporting wire, T_0 is the temperature of thermal bath and Q is the power provided by the heater. The heater power $Q(t)$ is equal to Q_0 during the heating portion and equal to zero during the cooling portion, respectively (see Fig. X). The heat capacity is measured as follows. Initially, the sample is in equilibrium with the thermal bath at temperature T_0 (phase I). Then, the heat Q_0 is provided until the temperature become stable, i.e. $dT/dt = 0$. This results in following equation

$$Q_0 = \kappa(T - T_0) \quad (\text{A-5})$$

which gives the magnitude of κ (phase II). Finally, the decay of temperature is measured by switching off the heater (phase III). The sample (platform) temperature can be expressed by following equation,

$$T = \Delta T \exp\left(-\kappa \frac{1}{C_{total}}\right) \quad (\text{A-6})$$

Here, κ/C corresponds to the relaxation time τ . Therefore the heat capacity C_{total} can be estimated by measuring the decay of temperature of the sample platform.

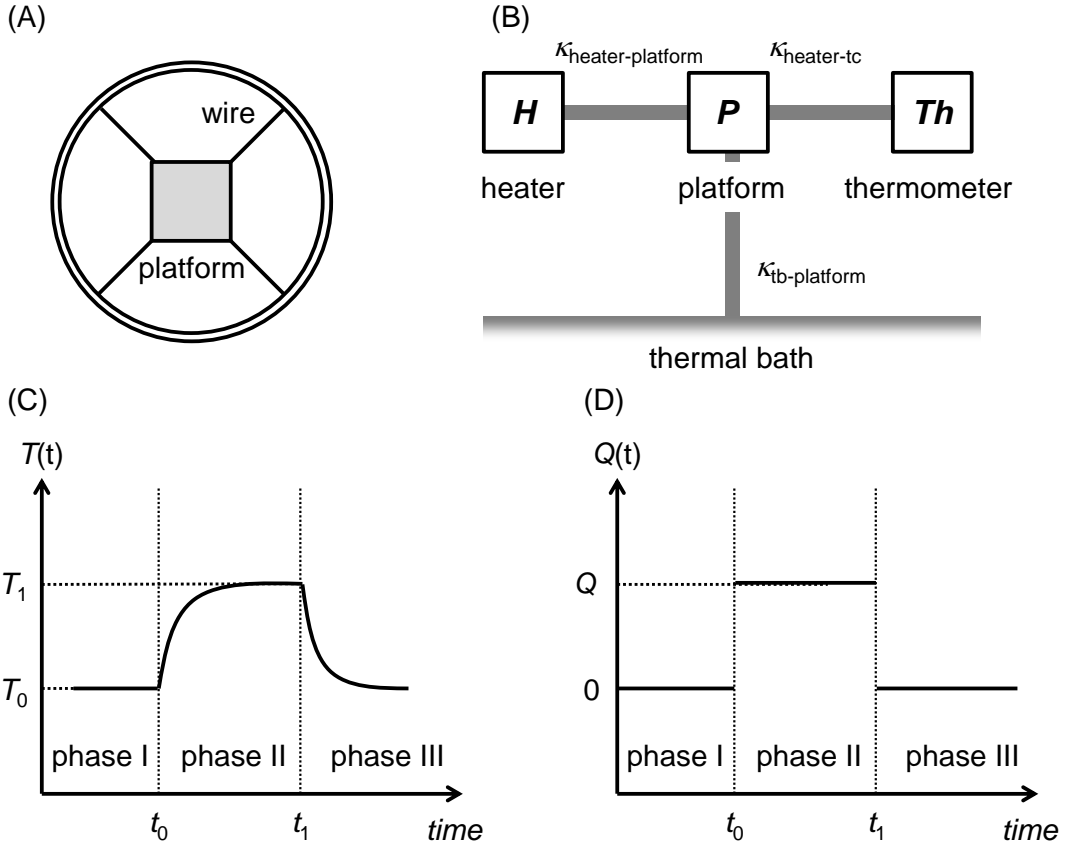


Figure A-2: (A) schematic picture of heat capacity sample puck and (B) thermal contact. (C) The temperature of sample puck as a function of time. The provided heat is summarized in (D). In phase I and III, no heat is provided into the system while the heat Q is provided into the system in the phase II.

Magnetic susceptibility of pure Ta_2NiSe_5 below T_c

Here we show the reported magnetic susceptibility of Ta_2NiSe_5 below 350 K. The data presented here shows anomaly-like behavior at approximately 100 K. However, we argue that the anomalies discovered in the old magnetic susceptibility data is not

originated from any phase transitions, but impurity effects. Fig. A-3 (B) shows the magnetic susceptibility of Ta_2NiSe_5 taken by using single crystals. No anomaly can be identified at corresponding temperature and therefore the anomaly-like feature is originated from impurity effect, possibly the phase transition of oxygen. The magnitude of magnetic susceptibility reported in the literature is $\chi = -0.135 \times 10^{-6} \text{ emu/g} = -1.1 \times 10^{-4} \text{ emu/mol}$ at 100 K while our measurement shows the magnetic susceptibility gives $\chi = -4.5 \times 10^{-3} \text{ emu/mol}$ which is 40 times different [42]. Since we measured the magnetic susceptibility of Ta_2NiSe_5 by using a single crystal with magnetic field applied along the b -axis, the diamagnetism might be overestimated.

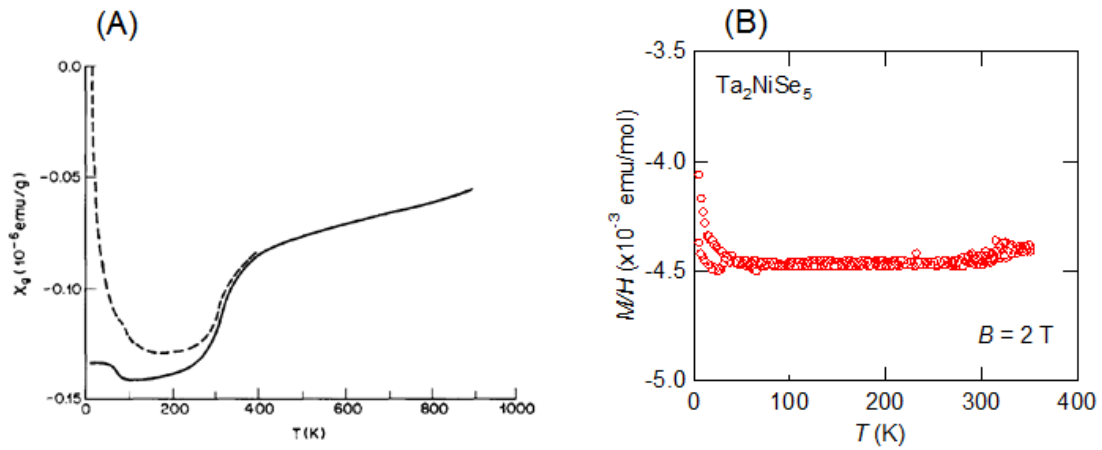


Figure A-3: (A) Magnetic susceptibility of Ta_2NiSe_5 as a function of temperature obtained by F. J. DiSalvo et al. and (B) our experiment. While an anomaly can be identified in the old experiment, no anomalies can be identified in our experimental data.

Acknowledgement

First, I would like to express my gratitude to Prof. H. Takagi for his excellent guidance, advice and encouragement during the course of my Ph. D. I am very much grateful to Dr. A. W. Rost and Dr. T. Takayama for their guidance and advices in the experiments. They always open door for my plenty of questions. During my Ph. D. and Master course, they supported my study in all the aspects such as experimental techniques, discussion about the results and how to give a presentation and writing in English. I could not complete my Ph. D. without their help. I thank to Dr. A. F. Bangura for his help of high field measurements. I thank to Dr. Y. Katsura for calculating band structure of Ta_2NiSe_5 and Ta_2NiS_5 which allow us to accurately understand the electronic structure of those materials. I would like to thank to Prof. Z. Hiroi, Prof. T. Shibauchi, Prof. T. Mizokawa, Prof. M. Yamashita and Prof. M. Lippma for giving me insightful comments and advices in my Ph. D. defense. I thank many students for discussion and refreshment, Mr. A. Kato, Mr. M. Nakamura, Mr. T. Yoshino, Mr. H. Kawasoko, Mr. H. Ishikawa, Mr. Y. Tashiro, Mr. Y. Yokota, Mr. K. Hayama, Mr. H. Kono and Ms. K. Shirai. Finally, I would like to thank my parents for their support and encouragement during my Ph. D course.

Yangfan LU
February 2015

Bibliography

- [1] J. H. de Boer and E. J. W. Verway, Proc. Phys. Soc. **49**, 59 (1937).
- [2] N. F. Mott and R. Peierls, Proc. Phys. Soc. **49**, 72 (1937).
- [3] J. G. Bednorz and K. A. Müller, Z. Physik B **64**, 189 (1986).
- [4] D. N. Basov and A. V. Chubukov, Nature Phys. **7**, 272 (2011).
- [5] E. Dagotto, T. Hotta and A. Moreo, Physics Reportes **344**, 1 (2001).
- [6] N. F. Mott, Phil. Mag. **6**, 287 (1961).
- [7] R.S. Knox, Solid State Phys. Suppl. **5**, 100 (1963).
- [8] W. Kohn, Phys. Rev. **19**, 439 (1967).
- [9] B. I. Halperin and T. M. Rice, Rev. Mod. Phys. **40**,755 (1967).
- [10] F. X. Bronold and H. Fehske, Phys. Rev. B **74**, 165107 (2006).
- [11] K. Seki, Y. Wakisaka, T. Kaneko, T. Toriyama, T. Konishi, T. Sudayama, N. L. Saini, M. Arita, H. Namatame, M. Taniguchi, N. Katayama, M. Nohara, H. Takagi, T. Mizokawa, Y. Ohta, Phys. Rev. B **90**, 155116 (2014).
- [12] H. Chia, T. Makino, K. Tamura, Y. Segawa, M. Kawasaki, A. Ohtomo and H. Koinuma, Appl. Phys. Lett. **82**, 1848 (2003).
- [13] J. Zittartz, Phys. Rev. **165**, 605 (1968).
- [14] D. Jerome, T. M. Rice and W. Kohn, Phys. Rev. **158**, 462 (1967).
- [15] J. A. Wilson, F. J. Di Salvo, and S. Mahajan, Phys. Rev. Lett. **32**, 882 (1974).
- [16] A. H. Castro Neto, Phys. Rev. Lett. **86**, 4382 (2001).
- [17] S. Giorgini, L. P. Pitaevskii, and S. Stringari, Rev. Mod. Phys. **80**, 1215 (2008).
- [18] P. Bhattacharyya and S. S. Jha, J. Phys. C: Solid State Phys. **11**, 805 (1978).
- [19] C Monney, G Monney, P Aebi and H Beck, New. J. Phys. **14**, 075026 (2012).
- [20] H. Cercellier, C. Monney, F. Clerc, C. Battaglia, L. Despont, M. G. Garnier, H. Beck, P. Aebi, L. Patthey, H. Berger, and L. Forro, Phys. Rev. Lett. **99**, 146403 (2007).
- [21] P. Wachter, J. Alloys and Comp. **225**, 133 (1995).
- [22] P. Wachter, Solid State Comm. **118**, 645 (2001).
- [23] B. Bucher, P. Steiner, and P. Wachter, Phys. Rev. Lett. **67**, 2717 (1991).
- [24] H. J. F. Jansen, A. J. Freeman and R. Monnier, Phys. Rev. B **31**, 4092 (1985).
- [25] P. Wachter and B. Bucher, Physica B, **408**, 51 (2013).
- [26] R. Suryanarayanan, G. Güntherodt, J. L. Freeouf, and F. Holtzberg, Phys. Rev. B **12**, 4215 (1975).
- [27] T. Matsumura, T. Kosaka, J. Tang, T. Matsumoto, H. Takahashi, N. Môri, and T. Suzuki, Phys. Rev. Lett. **78**, 1138 (1997).

- [28] H. Boppart, P. Wachter, B. Batlogg and R. G. Maines, *Solid State Comm.* **38**, 75 (1981).
- [29] F. Lapierre, P. Haen, B. Coqblin, M. Ribault and F. Holtzberg, *Physica* **108B**, 1351 (1981).
- [30] U. Kobler, K. Fischer, K. Bickmann and H. Lustfeld, *J. Mag. Mag. Mater.* **24**, 34 (1981).
- [31] F. Gronvold and F. J. Langmyhr, *Acta Chemica Scandinavia* **15**, 1949 (1961).
- [32] A. Zunger and A. J. Freeman, *Phys. Rev. B* **17**, 1839 (1977).
- [33] F. J. DiSalvo, D. E. Moncton and J. V. Waszczak, *Phys. Rev. B* **14**, 4321 (1976).
- [34] E. Moronsan, H. W. Zandbergen, B. S. Dennis, J. W. G. Bos, Y. Onose, T. Klimczuk, A. P. Ramirez and R. J. Cava, *Nature Phys.* **2**, 544 (2006).
- [35] N. Ogasawara, K. Nakamura and S. Takana, *Solid State Comm.* **31**, 873 (1979).
- [36] J. Voit, L. Perfetti, F. Zwick, H. Berger, G. margaritondo, G. Gruner, H. Hochst and M. Grioni, *Science* **290**, 501 (2000).
- [37] B. Bucher, T. Park, J. D. Thompson and P. Wachter, arXiv: 0802. 3354v2.
- [38] H. P. Hughes, *J. Phys. C: Solid State Phys.* **10**, 319 (1977).
- [39] K. Rossnagel, L. Kipp and M. Skibowski, *Phys. Rev. B* **65**, 235101 (2002).
- [40] L. F. Mattheiss, *Phys. Rev. B* **8**, 3719 (1973).
- [41] A. Sunshine and J. A. Ibers, *Inorg. Chem.* **24**, 3611 (1985).
- [42] F. J. DiSalvo, C. H. Chen, R. M. Fleming, J. V. Waszczak and R. G. Dunn, *J. Less-Common Metals* **116**, 51 (1986).
- [43] T. Kaneko, T. Toriyama, T. Konishi, and Y. Ohta., *Phys. Rev. B* **87**, 035121 (2013)
- [44] Y. Wakisaka, T. Sudayama, K. Takubo, M. Arita, H. namatame, M. Taniguchi, N. Katayama, M. Nohara and H. Takagi, *Phys. Rev. Lett.* **103**, 026402 (2009).
- [45] M. Moustafa, T. Zandt, C. Janowitz and R. Manzke, *Phys. Rev. B* **80**, 035206 (2009).
- [46] P. J. Squattritto, S. A. Sunshine and J. A. Ibers: *J. Solid State Chem.* **64** (1986) 261.
- [47] E. Canadell and M. H. Whangbo, *Inorg. Chem.* **26**, 3974 (1987).
- [48] D. J. Singh, *Phys. Rev. B* **88**, 174508 (2013).
- [49] Y. F. Lu, T. Takayama, A. F. Bangura, Y. Katusra, D. Hashizume and H. Takagi, *J. Phys. Soc. Jpn.* **83**, 023702 (2014).
- [50] N. R. Werthamer, E. Helfand and P. C. Hohenberg: *Phys. Rev.* **147** (1966) 295.
- [51] A. M. Clogston: *Phys. Rev. Lett.* **9** (1962) 266.
- [52] T. Coffy, C. Martin, C. C. Agosta, T. Kinoshota and M. Tokumoto, *Phys. Rev. B* **82** (2010) 212502.
- [53] H. Lei, R. Hu, E. S. Choi, J. B. Warren and C. Petrovic, *Phys. Rev. B* **81** (2010)

094518.

[54] I. J. Lee, M. J. Naughton, G. M. Danner and P. M. Chaikin, *Phys. Rev. Lett.* **78** (1997) 3555.

[55] K. Ishida, H. Mukuda, Y. Kitaoka, K. Asayama, Z. Q. Mao, Y. Mori and Y. Maeno, *Nature* **396**, 658 (1998).

[56] F. Hardy and A. D. Huxley, *Phys. Rev. Lett.* **94** (2005) 247006.

[57] T. P. Orlando, E. J. McNiff Jr, S. Foner and M. R. Beasley, *Phys. Rev. B* **19**, 4545 (1979).

[58] M. M. Altarawneh, N. Harrison, G. Li, L. Balicas, P. H. Tobasha, F. Ronning and E. D. Bauer, *Phys. Rev. Lett.* **108** (2012) 066407.

[59] R. E. Amritkar and N. Kumar, *Solid State Comm.* **26**, 627 (1978).

[60] L. E. Brus, *J. Chem. Phys.* **80**, 4403 (1984).

[61] C. Mailhot, Y. C. Chang, T. C. McGill, *Phys. Rev. B* **26**, 4449 (1982).

[62] S. Ishizawa, S. Kato, T. Maruyama and K. Akimoto, *Jpn. J. Appl. Phys.* **40**, 2765 (2001).

[63] E. J. H. Lee, C. Ribeiro, T. R. Giraidi, E. Longo, E. R. Leite and J. A. Varela, *Appl. Phys. Lett.* **84**, 1745 (2004).

[64] L. Li, W. Wang, X. Liu, Q. Song and S. Ren, *J. Phys. Chem. C* **113**, 8460 (2009).

